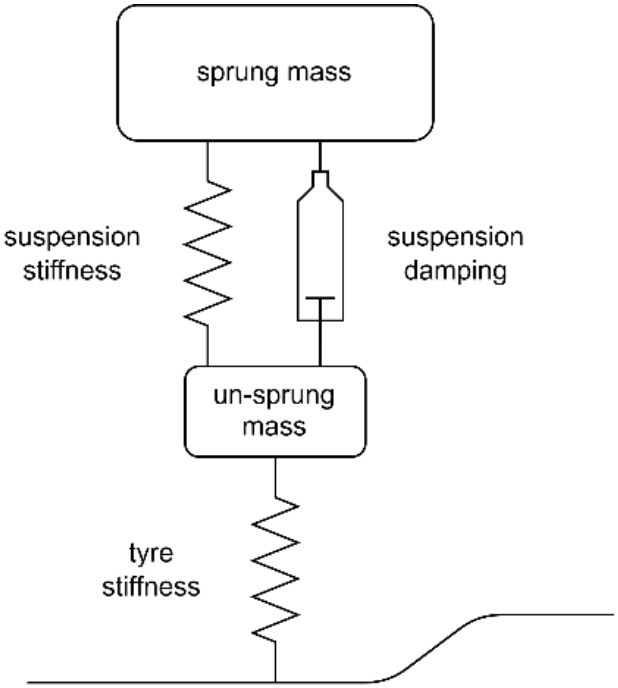

Suspension vertical and longitudinal modeling and parameter estimation for ride comfort assessment

Master's thesis in Mobility Engineering

SUMANTH PAI
MIGUEL GAMEZ BERRAL

DEPARTMENT OF MECHANICS AND MARITIME SCIENCES

CHALMERS UNIVERSITY OF TECHNOLOGY
Gothenburg, Sweden 2025
www.chalmers.se

Master's Thesis in Mobility Engineering

Suspension Vertical and Longitudinal Modeling and Parameter Estimation for Ride Comfort Assessment

SUMANTH PAI
MIGUEL GAMEZ BERRAL

CHALMERS
UNIVERSITY OF TECHNOLOGY

Department of Mechanics and Maritime Sciences
Division of Division Name
Chalmers University of Technology
Gothenburg, Sweden 2025

Suspension vertical and longitudinal modeling and parameter estimation for ride comfort assessment
SUMANTH PAI
MIGUEL GAMEZ BERRAL

Supervisor: Ajay Daniel, Volvo Cars AB
Examiner: Bengt Jacobson, Mechanics and Maritime Sciences, Chalmers

Master's Thesis 2025
Department of Mechanics and Maritime Sciences
Chalmers University of Technology
SE-412 96 Gothenburg
Sweden
Telephone +46 31 772 1000

Cover: Generic Quarter-Car model schematic.

Department of Mechanics and Maritime Sciences
Gothenburg, Sweden 2025

Modeling and Simulation of a suspension using a vertical and longitudinal combined quarter-car approach, evaluated with experimental data

SUMANTH PAI
MIGUEL GAMEZ BERRAL
Department of Mechanics and Maritime Sciences
Division of Division Name
Chalmers University of Technology

Abstract

Ride comfort is a key vehicle attribute, strongly influenced by suspension design and vital to both perceived quality and long-distance comfort. Setting meaningful requirements early in development is challenging, as engineers must work with aggregated vehicle parameters. Existing high fidelity simulation tools, while powerful, typically require detailed component data, limiting their usefulness in early-stage development. At the same time, increasing pressure from electrification and competition makes it more important than ever to define clear ride requirements early, to downstream effectively.

To address this challenge, this thesis investigates whether a simplified modeling approach can aid early-stage ride comfort target setting, focusing specifically on impact harshness. A modular quarter-car model was developed that includes both vertical and longitudinal dynamics, along with a simplified tire model to represent force distribution in both directions. Tailored for the concept phase, the model was structured around system-level inputs rather than detailed component data. To capture the relevant high-frequency dynamics, vertical parameters were identified using 4-poster shaker rig data through nonlinear optimization. Kinematics & Compliance (K&C) rig data supported both the estimation process and partial parameterization of the longitudinal model. Data from three different vehicles were used to ensure the model's robustness across varying suspension setups. The model was evaluated by simulating a cleat test and comparing its outputs with corresponding test track measurements.

The nonlinear optimization of vertical parameters allowed the model to capture ground-to-body acceleration with an average fit exceeding 80 percent across all vehicle axles. Impact harshness metrics predicted from cleat simulations showed deviations of up to roughly 50 percent across different axles, with some larger discrepancies in specific cases. These differences were primarily linked to the simplified tire model's limited ability to capture high-frequency dynamics.

Keywords: Suspension modeling, Quarter-Car, longitudinal suspension, NVH, ride comfort, impact harshness, Shaker rig, K&C rig, parameter identification

Acknowledgements

We would first like to express our sincere gratitude to our supervisor, Ajay Daniel, for his continuous guidance, valuable input, and active involvement throughout this thesis. His support and encouragement were crucial in shaping the direction of our work. We would also like to thank Axel Villandseie for generously sharing his experience and providing insightful advice that greatly helped us during the project. Furthermore, we are grateful to Sofia Kasimi, for facilitating the administrative processes and ensuring that everything ran smoothly, allowing us to focus on our work. A special thanks also goes to the Measurement Team at Hällered, whose structured approach and dedicated support in recording extensive amounts of data made an essential contribution to this thesis.

Finally, we would like to thank our academic supervisor, Bengt Jacobson, for his constructive feedback, valuable academic perspective, and guidance throughout the project.

Göteborg, October 2025

SUMANTH PAI, MIGUEL GAMEZ BERRAL

List of Acronyms

Below is the list of acronyms that have been used throughout this thesis listed in alphabetical order:

FBD	Free Body Diagram
SPMM	Suspension Parameter Measuring Machine
K&C	Kinematics & Compliance
SF	Sub-frame
TM	Top Mount
PWT	Powertrain
IH	Impact Harshness
PSD	Power Spectral Density
ODE	Ordinary Differential Equation
RMS	Root Mean Square
VDV	Vibration Dosage Value
MBD	Multi Body Dynamics

Contents

1

Introduction

Ride comfort is a key performance attribute in vehicle development, affecting both perceived quality and long-distance comfort. In the early concept phase of vehicle development, detailed suspension information—such as hardpoint locations, damper curves, or tire models—is usually not yet defined. Instead, engineers work with aggregated representations like axle targets a.k.a virtual design parameters, which describe desired vehicle behavior at a higher level. These targets help guide early design choices without relying on specific component details. As development progresses and subsystem-level data becomes available, high-fidelity tools like Multi-Body Dynamics (MBD) simulations become more effective. These tools require accurate suspension geometry and component characteristics, and are better suited for later stages when detailed tuning and validation of ride comfort are needed [1].

However, optimizing ride comfort is inherently complex. It requires balancing the need for smoothness with the demands of handling performance—two objectives that often conflict. When evaluating ride, engineers must consider how vibrations travel through the vehicle's suspension, tires, and body structure before reaching the driver and passengers. These vibrations span a wide frequency range and are typically categorized into three domains: primary ride (low-frequency body motions), secondary ride (mid-frequency vibrations), and impact harshness (high-frequency, short-duration shocks).

These three domains of ride correspond to different parts of the vibration spectrum and require tailored evaluation strategies. However, assessing ride quality across these ranges is particularly challenging during early development, when detailed component data and physical prototypes are not yet available to support high-fidelity simulations.

Once prototypes are built, engineers evaluate ride behavior using a combination of real-world testing and controlled laboratory setups, such as 4-poster rigs. These methods help quantify vehicle response to various frequency inputs and are often used alongside standardized evaluation frameworks, such as ISO 2631-1. This standard provides objective metrics—like Root Mean Square (RMS), Vibrational Dosage Value(VDV) that capture different aspects of vibration severity and human perception.

This thesis focuses on impact harshness, which is especially important for perceived

quality but difficult to address early in the design phase due to the complexity of full-vehicle modeling.

1.1 Background

Ride comfort is a critical performance attribute in vehicle development, influencing both perceived quality and long-distance driving comfort. It is often evaluated using advanced simulation tools such as Multi-Body Dynamics (MBD) software, which require detailed modeling of suspension kinematics, damping behavior, and full-vehicle responses. These tools are highly effective during later development stages, when accurate component-level data—such as suspension geometry, tire stiffness, and damper characteristics—are available. However, in the early concept phase, many of these parameters are either undefined or only loosely estimated. As a result, MBD models at that stage may lack the fidelity needed to make meaningful predictions about ride behavior, particularly in the higher-frequency domains associated with secondary ride and impact harshness.

Once physical prototypes are built, engineers gain access to objective test data that can be used to study ride behavior more concretely. Among the commonly used testing methods is the 4-poster shaker rig, which applies controlled vertical inputs at each wheel to simulate road excitations in a repeatable laboratory setting. These tests are valuable for evaluating vertical ride characteristics and tuning components during development. However, their applicability to high-frequency impact phenomena is limited. This is due to two key factors: (1) the inputs are purely vertical and do not involve realistic tire–road rolling interactions (combined vertical and longitudinal motion), and (2) the actuator systems are often bandwidth-limited, making it difficult to replicate sharp, high-frequency disturbances like potholes or expansion joints—typical of impact harshness scenarios.

Despite its limitations, the data obtained from 4-poster shaker rig testing, when combined with on-road test measurements, can still yield valuable insights into how vehicles respond to road inputs across a range of frequencies. This thesis adopts a quarter car modeling approach to leverage such existing objective data from past vehicles or prototypes. The goal is to parameterize a simplified, multi-degree-of-freedom ride model that supports the early definition of performance targets for impact-related behaviors at a stage where detailed simulation models are not yet feasible. In doing so, the work aims to bridge the gap between early concept decisions and the later validation stages of ride development.

1.2 Purpose

The purpose of this thesis is to explore whether a simple model can aid in setting axle level targets to meet vehicle impact harshness requirements early in the vehicle development process. Considering the extensive time and effort required for full Multi-Body-Dynamics(MBD) simulations, this study aims to assess whether a simplified approach, leveraging existing objective test data from previous vehicles or

competitors, can provide meaningful guidance. The focus is on developing an efficient tool to establish design targets that capture key ride behavior characteristics, particularly in high-frequency ranges. By doing so, the research seeks to bridge the gap between early-stage development and final validation, enabling a more streamlined approach to vehicle ride comfort optimization.

1.3 Objective

The objective of this thesis is to develop a simplified vehicle ride model that captures key dynamic behaviors associated with secondary ride and impact harshness. The model will incorporate multiple degrees of freedom in both the vertical and longitudinal directions, which is essential for representing the vehicle's response to high-frequency and high-amplitude inputs.

The main objectives of the project are to:

- Develop a simplified model with parameters suitable for early-phase vehicle development, and a modular structure that allows variations based on axle architecture.
- Integrate vertical and longitudinal dynamics to better represent impact responses.
- Use objective data from physical measurements—such as 4-poster shaker rig tests and on-road testing—for model parameter calibration and validation.
- Evaluate the model's ability to reproduce characteristic ride behaviors in the high-frequency domain.
- Implement the vertical parameter estimation from 4-poster shaker rig experiments as a useful tool in python.

The ultimate aim is to demonstrate a simplified modeling methodology that supports early-stage ride comfort target setting, particularly in the high-frequency domain, before detailed simulation or physical testing is feasible.

1.4 Limitations

This thesis focuses only on impact harshness—short, high-frequency bump in the vertical and longitudinal directions. Other ride types, like primary ride (low-frequency) and secondary ride (mid-frequency), are not studied. So, the results should not be seen as a full assessment of overall ride comfort.

The model does not account for longitudinal forces resulting from propulsion or braking torques. Since the focus is on impact harshness at constant speed, those loads were considered outside the scope of this simplified early-phase model.

This work models only a single suspension corner and does not account for differences in motion between the left and right sides of the vehicle. While this limits the model's

ability to represent full-vehicle behavior, it is consistent with its intended use as a simplified tool for evaluating impact harshness in early design stages.

The model is intentionally simplified to support fast iterations and low computational demand for the early concept phase. It is not intended to replace high-fidelity simulation tools like Multi-Body Dynamics (MBD) in later development stages. The simplification includes aggregated parameters and assumptions that may not hold as detailed component data becomes available. Details such as anti-dive or other kinematic parameters are not modeled.

The model is designed to predict relative changes in ride performance in response to parameter variations, rather than absolute ride metrics. As such, it is most effective for early-stage design target setting for example, comparing axle configurations or estimating sensitivity to stiffness changes rather than making definitive performance predictions. Model results should be interpreted accordingly and supplemented with more detailed analysis as development progresses.

2

Theory

Ride comfort refers to how smooth and comfortable a vehicle feels when driving, especially in response to road irregularities. It is mainly influenced by how the vehicle moves over different types of surfaces and how those movements are transmitted to the passengers. These motions create vibrations, which are felt in the cabin and directly impact the perceived comfort. Although comfort is subjective, it can be studied using measurable physical quantities such as acceleration and frequency [12].

Human sensitivity to vibrations depends largely on frequency. As noted by Heissing and Ersoy [12], low-frequency vibrations around 0.5–0.75 Hz can cause motion sickness, while mid-range frequencies from 3–11 Hz affect the torso and internal organs. Vibrations near 25 Hz tend to affect the head and neck area. This sensitivity range helps define how vibrations impact ride comfort and why certain frequencies are more critical to control in vehicle design.

To better analyze and improve ride quality, the response of a vehicle to road-induced inputs is typically divided into three categories: primary ride, secondary ride, and impact harshness [11, 12].

Primary ride involves low-frequency motions, generally from 0 to 3–4 Hz. These are related to the large-scale movements of the vehicle body, like bounce, pitch, and roll. These motions are mainly controlled by the suspension system and are influenced by the vehicle's response to larger road undulations.

Secondary ride refers to mid-frequency vibrations, typically ranging from 3 Hz to around 20–50 Hz, depending on the literature. These are caused by smaller bumps and surface irregularities, and are linked more to the unsprung mass and finer details of the suspension system. This type of ride affects the vehicle's smoothness and overall refinement.

Impact harshness is usually associated with the higher end of the secondary ride frequency range (around 20–50 Hz). It relates to sharp, short-duration inputs like potholes or road joints. These are felt as sudden jolts and are often considered separately due to their effect on the perceived quality of the ride [14].

Engineers often use tools like accelerometers to measure vibrations and analyze them using methods such as power spectral density (PSD) to understand how they are distributed across different frequencies [13]. Although these measurements are

objective, the final judgment of ride quality still depends on how passengers perceive the vehicle's behavior.

2.1 Impact scenario

Impact harshness refers to the vehicle's immediate and intense response when encountering a sudden road disturbance—such as a cleat, bump, or pothole—typically at moderate speeds around 30 km/h. This scenario is often evaluated through controlled tests where the vehicle is driven over standardized obstacles, and acceleration data is recorded at key locations like the seat rail or chassis. The resulting vibration profile is analyzed in two parts: the initial impact response, which captures the sharp, high-magnitude acceleration occurring within the first 100 milliseconds, and the aftershake, a lower-magnitude oscillation that follows. These metrics help engineers assess both the severity of the impact and the vehicle's ability to settle quickly. As the tire rolls over the obstacle, it initiates a chain of dynamic force transmission through the vehicle's load path—including the wheel assembly, suspension links, subframe, and body mounts. Each of these components plays a role in modulating the disturbance. Tires and compliant elements like rubber bushings help absorb high-frequency content, while the suspension's mass, stiffness, and damping characteristics determine how effectively the system isolates the vehicle body. Understanding how these forces propagate and are attenuated along this path is essential for designing vehicles that minimize harshness and enhance occupant comfort.

2.1.1 Tire interaction

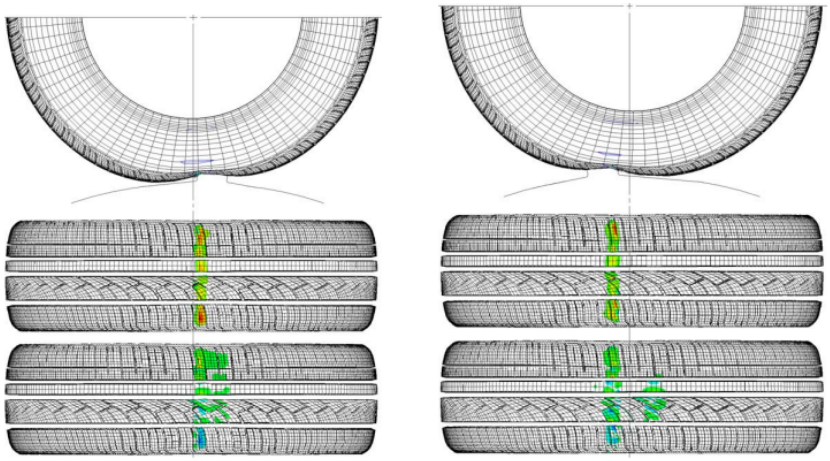

Figure 2.1: Normal & tangential stress contours before and after impact [2]

The study done by Cho et al.[2] studied the transient dynamic response of a rolling tire with a small cleat using an FEM model and comparing it to experimental data. In this work, a detailed 3D finite element model of a patterned tire was developed to simulate the localized interaction between the tire tread and a rigid cleat. The

simulation captured both the time-history and frequency-domain responses of the dynamic forces at the tire axis, offering insight into how such impacts translate into vehicle excitations. The model results were validated against experimental data, showing strong agreement, and a parametric investigation revealed how tire rolling speed and inflation pressure influence the transient response characteristics.

2.2 Suspension systems

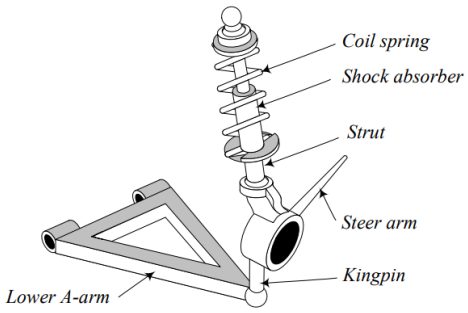

Figure 2.2: McPherson [8]

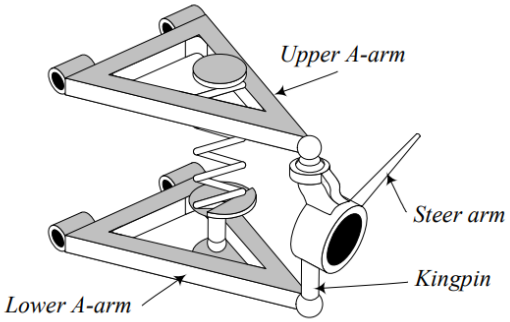

Figure 2.3: Double wishbone [8]

The suspension system is the next major component in the load path after the tire, and it plays a central role in determining how forces are transmitted to the chassis. The layout of the suspension defines this load path and influences how inputs are distributed across the vehicle structure. Common front suspension configurations include the McPherson strut and the double wishbone or multi-link setup. As can be seen in the figure above. In a McPherson layout, the damper is mounted directly to the knuckle, allowing vertical forces from the wheel to be transmitted directly to the chassis. In contrast, in double wishbone or multi-link systems, the damper is mounted to the lower control arm. This arrangement introduces a lever effect, where the force from the wheel is transmitted through the arm to the damper, resulting in increased reaction forces at the damper mount and higher dynamic loads on the subframe. The stiffness and mass of the subframe, as well as the compliance of its bushings, become important factors in how effectively these forces are managed.

The wheel rate signifies the effective vertical stiffness of the suspension system as experienced at the wheel. It describes how much force is needed to vertically displace the wheel by a given amount, accounting not only for the spring stiffness but also for the suspension geometry. This makes wheel rate a more accurate representation of the suspension's behavior under real-world road inputs than the spring rate alone. The wheel rate is calculated using the formula:

$$k_{wheel} = (Motionratio)^2 * k_{spring}$$

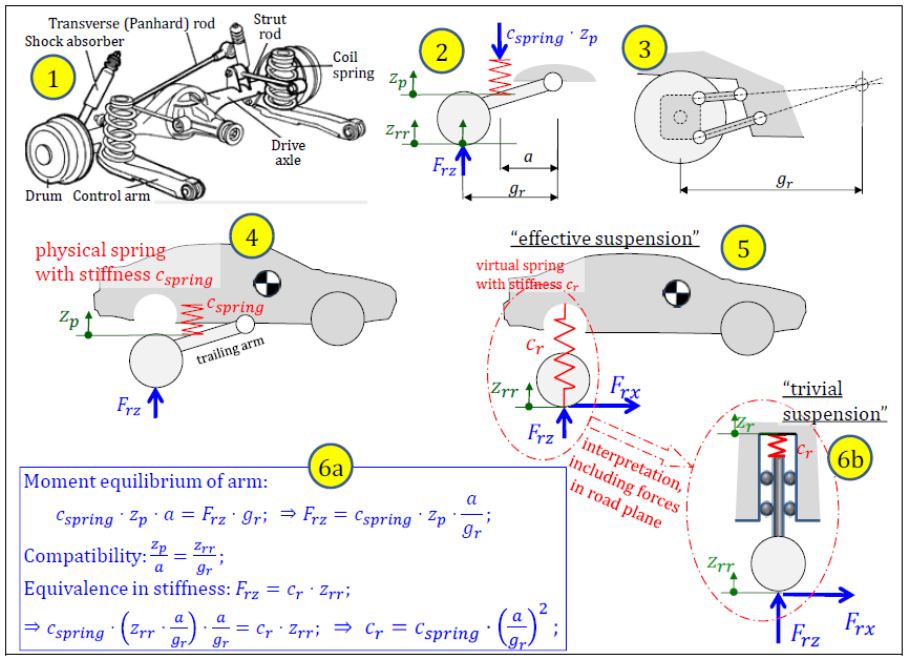

Figure 2.4: Wheel rate formulation [6]

Referring to the image above from the compedium, the motion ratio is defined as the ratio of spring displacement to wheel displacement. In idealized 2D example shown above, this ratio can be computed analytically using basic geometry. However, for realistic suspension systems, especially those with non-linear motion paths or complex kinematics (e.g., double wishbone or multi-link setups), the motion ratio is best determined using 3D modeling or multibody dynamics (MBD) simulation tools. These tools capture the full geometric and kinematic behavior of the system, allowing for accurate estimation of motion ratios across the suspension's range of motion.

2.2.1 Bushings

Bushings, typically made of rubber, are essential components in modern suspension systems. They serve as flexible joints that connect suspension parts to each other, to the subframe, and to the vehicle body. Their main role is to isolate the chassis from road-induced vibrations and shocks, improving ride comfort without compromising structural integrity. Soft, compliant bushings are effective at filtering out high-frequency disturbances, making them ideal for comfort. However, stiffer bushings are often used to improve handling, as they reduce unwanted movement between suspension components. This movement, if not controlled, can alter suspension geometry under dynamic conditions like braking or cornering—a phenomenon known as elasto-kinematic behavior. While this effect can influence handling, it is often used intentionally in modern vehicle design to fine-tune dynamic performance[12]. The mechanical behavior of bushings is complex and nonlinear, influenced by factors such as displacement, frequency, preload, and temperature. In most cases, stiffness changes with displacement are the dominant factor, but other influences become

more important under dynamic conditions[12].

2.2.1.1 Damper bushing

The interface between the damper and the body is often characterized by a soft connection through a rubber bushing. This bushing, positioned between the damper and the vehicle body, introduces a compliant interface that significantly influences how damping forces are transmitted. Instead of acting as a rigid connection, it provides nonlinear compliance that alters the damper's behavior depending on the displacement amplitude.

At small displacement amplitudes, which are typically associated with high-frequency and low-energy road inputs, the bushing absorbs part of the motion. This reduces the vibration transmitted to the vehicle body and enhances ride comfort on smoother surfaces where fine disturbances are more common.

In contrast, during larger suspension movements caused by body roll, pitch, or major road irregularities, the bushing's influence is reduced due to its limited deflection range. Under such conditions, the damper operates closer to its full capacity and delivers the required damping force to manage body motion effectively.

This amplitude-sensitive behavior creates a form of stroke-dependent damping. It offers a softer response to minor inputs while preserving stiffness and control for more significant dynamic events. As a result, the damper bushing plays a key role in balancing comfort and handling by modulating the force transfer between the suspension and the vehicle body [5].

2.2.1.2 Engine mount bushings

In most modern vehicles, the engine and transmission are treated as a single powertrain unit, mounted to the vehicle body using a combination of engine mounts, transmission mounts, and torque supports [12]. These mounts are typically composed of bonded rubber-metal bushings, ranging from simple elastomeric types to more complex hydraulic or active mounts, depending on the vehicle class and NVH targets.

The primary reason bushings are used in powertrain mounts is their ability to support the engine's static weight while controlling its dynamic behavior. A rigid connection would transmit excessive vibrations and noise into the vehicle body, so bushings are used to provide:

- support under static and quasistatic loads,
- damping of low-frequency, high-amplitude engine motions,
- isolation of high-frequency, low-amplitude excitations to improve cabin comfort.

These functions are especially important given that engine-induced vibrations span a wide frequency range, and must be tuned carefully to avoid resonances within

the chassis or suspension system. The bushings allow the engine/transmission unit to perform small translational and rotational movements, forming a spring-mass-damper system with the mounts. This setup not only controls the displacement due to load shifts or torque reactions, but also reduces structure-borne noise, especially at high frequencies.

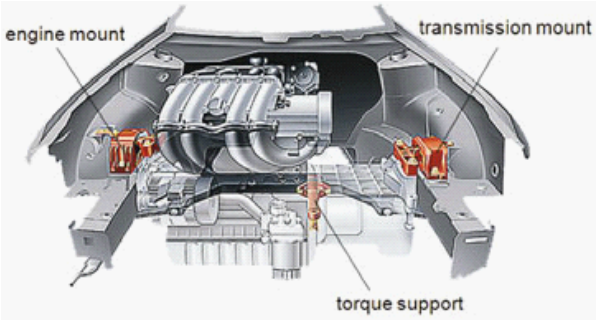

Figure 2.5: Combustion engine transverse layout engine mounts location [12]

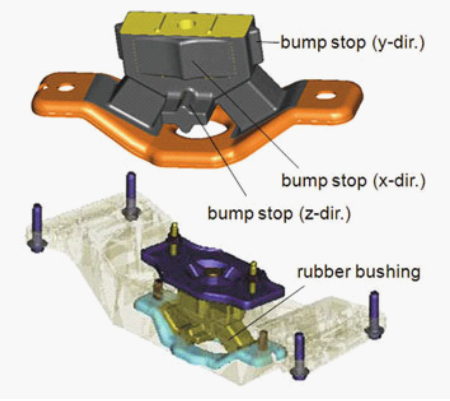

Figure 2.6: conventional engine mount [12]

Hydraulic engine mounts are widely used in modern vehicles to further enhance vibration isolation. These mounts include an internal fluid-filled chamber separated into two working volumes by a tuned channel system. When dynamically excited, fluid is pumped between the chambers, producing frequency-selective damping. This system enhances isolation in the lower frequency range while increasing dynamic stiffness at higher frequencies, reducing issues like body shudder.

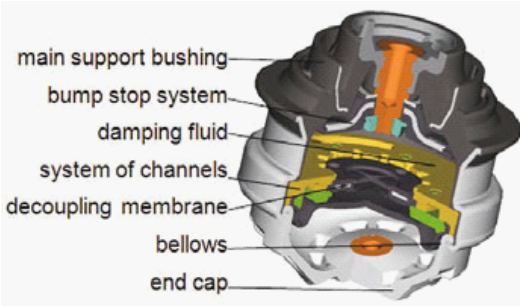

Figure 2.7: Hydraulic engine mount [12]

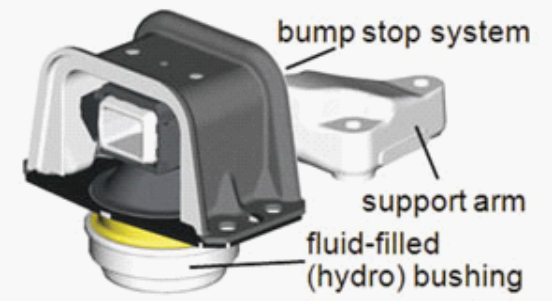

Figure 2.8: Hydraulic engine mount with support [12]

To manage the dynamic behavior of hydraulic mounts without introducing excessive stiffness across all frequencies, a decoupling mechanism is integrated between the fluid chambers. The fluid-filled chamber is divided into two working volumes connected by geometrically-tuned channels. Under dynamic excitation, fluid is pumped between these chambers, generating frequency-selective damping. This behavior is characterized by parameters such as the loss angle and dynamic stiffness, whose frequency-dependent behavior is shown in Figure 2.9.

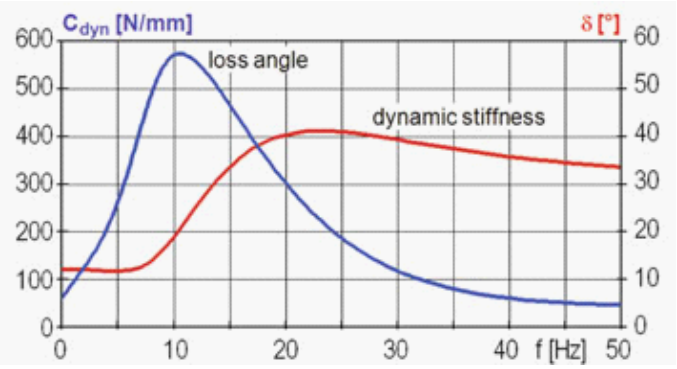

Figure 2.9: Transfer function of a hydraulic engine mount

Hydraulic damping tends to increase the mount's dynamic stiffness in the mid to high-frequency range, which improves vehicle stability and suppresses shudder. However, to maintain good isolation at lower frequencies—where acoustic sensitivity is highest—a decoupling system is introduced to reduce fluid flow resistance at those frequencies. This allows engineers to tune the mounts to both suppress resonances, particularly near 10Hz in the vertical direction, and maintain occupant comfort. Thus, hydraulic mounts help achieve a balance between ride comfort and handling performance, even under small excitation amplitudes.

2.2.1.3 Subframe bushings

Chassis subframe bushings play a crucial role in isolating road and powertrain-induced vibrations from the vehicle body, thereby enhancing ride comfort and reducing cabin noise [12]. By mounting the axle or powertrain onto a subframe that is itself elastically connected to the chassis, these mounts absorb high-frequency vibrations through their inherent damping characteristics and the subframe's inertial mass.

These bushings are typically designed with directional stiffness characteristics: high lateral stiffness ensures handling precision, while softer longitudinal and vertical stiffness promotes comfort and noise isolation. To achieve this, subframe bushings are often large in size (typically 70–100 mm in diameter) and use soft, elastic rubber materials. The internal design—including the shape of the rubber and the contour of the inner core—allows for tunable stiffness in specific directions.

The configuration also provides assembly benefits: the axle or powertrain can be preassembled as a module and mounted onto the vehicle, simplifying production. In most cases, the bushings include a rubberized outer sleeve that compensates for manufacturing tolerances and facilitates press-fit assembly without the need for precise surface finishing.

Because these mounts carry substantial loads—such as the engine weight, control forces from the suspension, and part of the vehicle mass—their preload under static weight can cause significant compression and long-term setting. Therefore, the design must account for axial deflection to maintain adequate vertical travel and system

compliance.

To balance vibration isolation and structural control, hydraulically-damped subframe bushings are often used. These feature internal chambers and channel systems that provide frequency-dependent damping, which is particularly useful for tuning ride and handling in high-performance or premium-class vehicles. Axial and radial displacements are controlled through bump stops and limiter plates integrated into the bushing geometry.

Here below are some examples of subframe bushings.

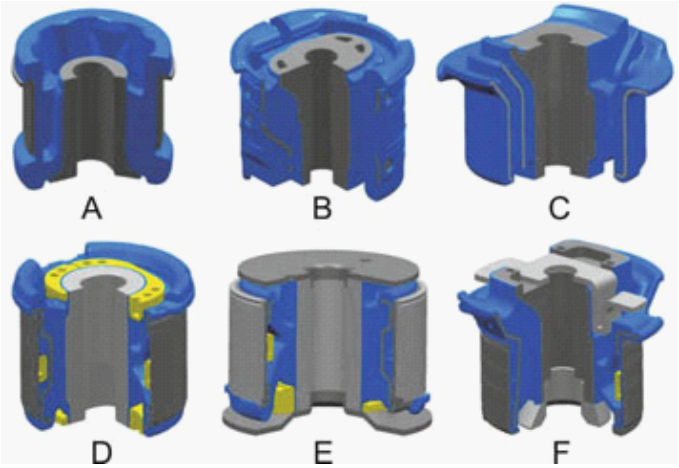

Figure 2.10: Conventional and hydraulically-damped chassis subframe mount designs [12]

2.3 Suspension models

In the study of vehicle ride dynamics, selecting an appropriate modeling approach is crucial and depends largely on the specific objectives and the level of data available.

The *quarter car model* is the most basic form, consisting of a single wheel, its suspension system, and the associated portion of the vehicle body (sprung mass). This model is particularly effective for analyzing vertical dynamics and is commonly used for early-stage studies of suspension damping and ride comfort.

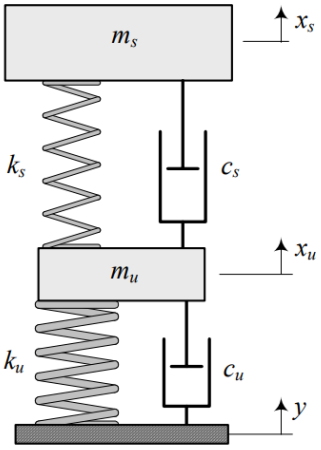

Figure 2.11: Standard quarter car model [8]

The *half-car model* extends this representation by including both front and rear suspension systems, thereby introducing pitch motion. This allows engineers to assess how vehicle ride is influenced by longitudinal dynamics, such as during braking or acceleration.

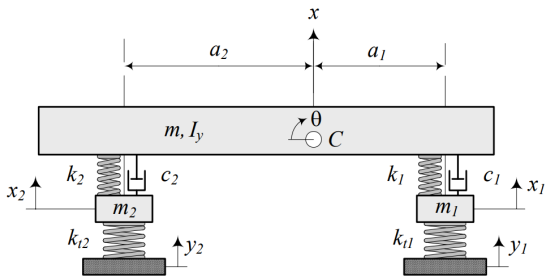

Figure 2.12: Half car model [8]

The *full-car model* further expands the system to include all four suspension corners, enabling the analysis of vertical (heave), pitch, and roll motions simultaneously. This model is suitable for evaluating whole-body dynamic responses and cross-corner interactions under road excitations.

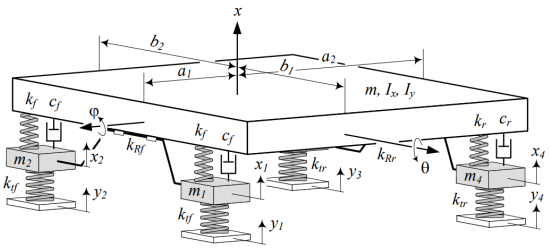

Figure 2.13: Full car model [8]

At the highest fidelity, *multi-body dynamic (MBD)* models are employed to simulate real-world behavior with detailed suspension geometries, non-linear damping, and three-dimensional vehicle motion. These models require extensive input data and computational resources, making them most appropriate for advanced development stages where component-level information is well-defined.

Each model presents a trade-off between computational simplicity and physical realism for different driving maneuvers. Therefore, the choice of modeling approach should be guided by the intended application, available data, and the phase of the vehicle development process.

2.3.1 Sprung mass assumption in quarter car vertical & Longitudinal Models

While quarter-car models simplify suspension analysis by isolating a single wheel's dynamics, it's important to consider how mass representation differs between vertical and longitudinal directions.

In the vertical direction, disturbances from the road typically act far from the vehicle's center of gravity (CoG), often inducing pitch motion. This means the effective mass experienced at a suspension corner may be greater than one-fourth of the total sprung mass. However, for simplicity, vertical quarter-car models often assign exactly one-fourth of the sprung mass per wheel, effectively decoupling pitch and focusing only on local vertical motion.

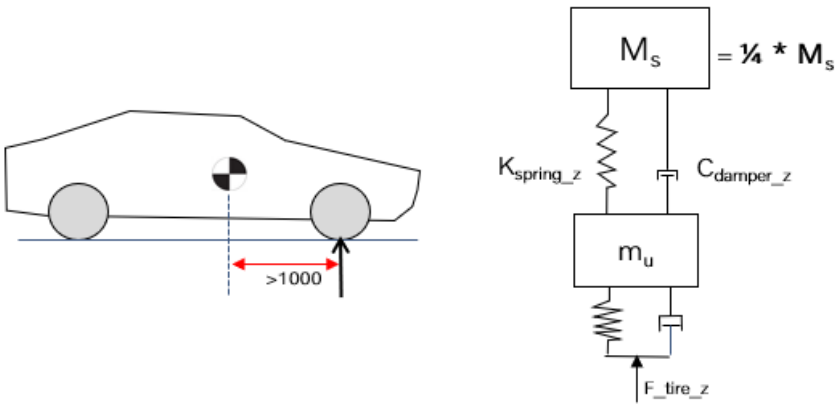

Figure 2.14: Quarter car vertical

In the longitudinal direction, the input from an event such as a vehicle hitting a cleat or a steep bump occur near the CoG in the vehicle longitudinal axis. As a result, pitch effects are minimal. Therefore, when analyzing a single wheel/quarter car, it is often reasonable to consider that roughly half the total sprung mass (e.g., the left or right side of the vehicle) contributes to the longitudinal dynamics at that corner.

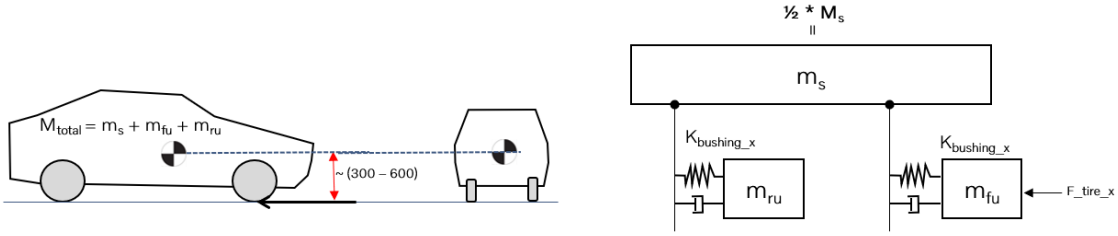

Figure 2.15: Quarter car longitudinal

2.3.2 Powertrain mass & top mount bushing influence

As discussed in Section 2.2.1.1, the damper's connection to the vehicle body is typically made through a rubber bushing known as a top mount. The research conducted by Bennett [15] highlights the importance of modeling this component, which is often overlooked in simplified suspension models. Bennett performed a sensitivity analysis by systematically varying the top mount stiffness in both single-path and dual-path configurations. His study showed that the top mount significantly influences both the impulse and frequency responses of the suspension system. Specifically, variations in stiffness impacted the system's dynamic stiffness and damping behavior, especially around the hub mode frequency. The findings concluded that excluding the top mount can result in under-prediction of key suspension characteristics, emphasizing its critical role in realistic and accurate vehicle dynamic modeling.

In simplified vehicle models, it is often assumed that components such as the engine, exhaust system, and other assemblies connected to the sprung mass are rigidly mounted. However, in reality, these components are typically attached using flexible mountings, which contribute dynamic behaviour that is frequently overlooked. According to Bennett[15], the natural frequencies of these suspended subsystems commonly fall within the 0.5 to 40Hz range, which coincides with the frequency band investigated through four-post rig testing. His study, which examined a front-wheel-drive combustion vehicle, highlights the significance of accounting for engine mass by analysing the apparent sprung mass response across frequency. The results show that resonance effects near 7Hz, if not properly modelled, can lead to substantial errors in representing the vehicle's dynamic behaviour, particularly at the front end where the engine is located.

2.4 Modeling of different connecting elements

2.4.1 Damper modeling

The modelling of automotive dampers, or shock absorbers, is a critical aspect of vehicle dynamics due to their significant influence on ride comfort and handling. There are two approaches to modelling dampers: physical modelling and nonparametric (or empirical) modelling [17].

2.4.1.1 Physical modeling

This approach is based on the internal structure and working principles of the damper. It involves the detailed representation of components such as valves, orifices, fluid compressibility, and mechanical constraints. While physical models provide high accuracy over a wide range of operating conditions, they are computationally expensive and require many parameters, some of which can only be obtained through specialized equipment. These models are useful for studying design changes but are impractical for real-time vehicle simulations.

2.4.1.2 Nonparametric modeling

Nonparametric or data-driven models use experimental data to define the relationship between damper input (usually piston velocity) and output (damping force), without assigning physical meaning to parameters. These models are more computationally efficient and can be easily fitted to test data using regression techniques. This makes them ideal for integration in vehicle simulation environments, particularly when full physical characterization is not feasible.

In the study by Cui et al. (2010), several damper models were proposed and evaluated using experimental data from a shock absorber tested on a single-post shaker rig. The damper was characterized over a velocity range of 0.01 m/s to 1.3 m/s using sinusoidal excitation. Among the modelling approaches considered were:

2.4.1.2.1 Linear model

The damping force is proportional to velocity:

$$F = c \cdot v \tag{2.1}$$

This simple model does not capture nonlinearities or hysteresis but serves as a basic reference.

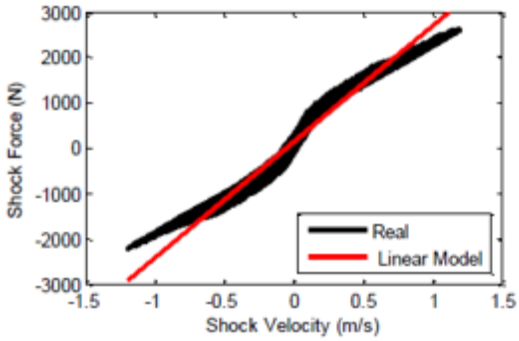

Figure 2.16: Linear damper model versus measurement

2.4.1.2.2 Segmented polynomial model

Polynomials are fitted to different velocity segments to accurately model the nonlinear and hysteretic force-velocity relationship. Fourth- and third-order polynomials were used for rebound and compression regions, respectively.

For rebound

$$F(v)=\begin{cases} a_{42}v^2+a_{41}v+a_{40} & 0<v\le v_4 \\ a_{54}v^4+a_{53}v^3+a_{52}v^2+a_{51}v+a_{50} & v>v_4 \end{cases}$$

and, for compression

$$F(v)=\begin{cases} a_{14}v^4+a_{13}v^3+a_{12}v^2+a_{11}v+a_{10} & v\le v_1 \\ a_{22}v^2+a_{21}v+a_{20} & v_1<v\le v_2 \\ a_{34}v^4+a_{33}v^3+a_{32}v^2+a_{31}v+a_{30} & v_2<v\le 0 \end{cases}$$

Figure 2.17: Polynomials

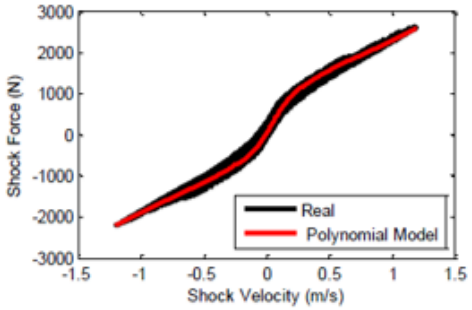

Figure 2.18: Model vs measurement

The study found that the polynomial model generally showed improved accuracy compared to the linear model in terms of root mean square (RMS) error when evaluated against experimental data. This model was better able to approximate the nonlinear and asymmetric characteristics of the damper.

Validation with sinusoidal inputs of varying frequency and amplitude indicated that the models captured key aspects of damper behavior, such as differing response between compression and rebound. While the models did not fully characterize all hysteresis effects observed in real shock absorbers, the segmented polynomial approach was presented as a practical option for representing damper dynamics in vehicle simulation environments, particularly when computational efficiency and ease of parameter fitting are important.

2.4.2 Bushing modeling

Bushings in suspension systems exhibit viscoelastic behavior, meaning they have both elastic (spring-like) and viscous (damper-like) properties. Accurately modeling this behavior is essential for representing how forces are transmitted and dissipated through suspension components. Several classical models have been developed to describe viscoelasticity, including the Maxwell model, the Kelvin–Voigt model, and the Standard Linear Solid model [18].

2.4.2.1 Maxwell model

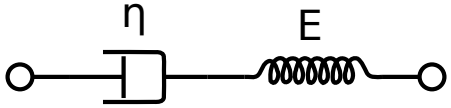

Figure 2.19: Maxwell model: spring and damper in series [18]

The Maxwell model consists of a spring and a damper connected in series. In this configuration, the total strain is the sum of the strains in the spring and the damper, while the stress is the same across both elements:

$$\varepsilon = \varepsilon_s + \varepsilon_d, \quad \sigma = \sigma_s = \sigma_d$$

Differentiating this relationship yields:

$$\dot{\varepsilon} = \frac{\sigma}{\eta} + \frac{\dot{\sigma}}{E}$$

Here, E is the elastic modulus of the spring, and η is the viscosity coefficient of the damper.

Under a constant applied stress, this model predicts a linearly increasing strain over time, corresponding to a constant strain rate. This implies that the stress response is independent of strain magnitude, which oversimplifies the behavior of real viscoelastic materials that typically exhibit a decreasing strain rate under constant stress (creep behavior).

2.4.2.2 Kelvin–Voigt model

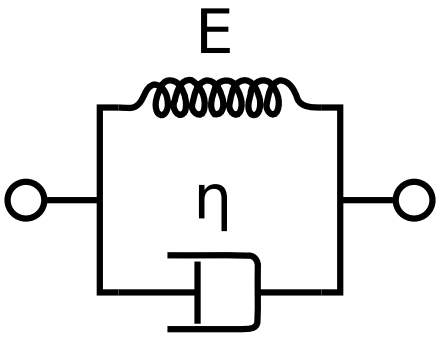

Figure 2.20: Kelvin–Voigt model: spring and damper in parallel [18]

The Kelvin–Voigt model, in contrast, arranges the spring and damper in parallel. In this setup, the strain is the same in both elements, and the total stress is the sum of their individual contributions:

$$\varepsilon = \varepsilon_s = \varepsilon_d, \quad \sigma = \sigma_s + \sigma_d$$

Leading to the constitutive equation:

$$\sigma = E \cdot \varepsilon + \eta \cdot \dot{\varepsilon}$$

This model prevents immediate deformation under a step load and accurately represents creep behavior, where strain increases gradually under constant stress. However, it does not account for stress relaxation—a common phenomenon where stress decreases over time under constant strain.

2.4.2.3 Standard linear solid model

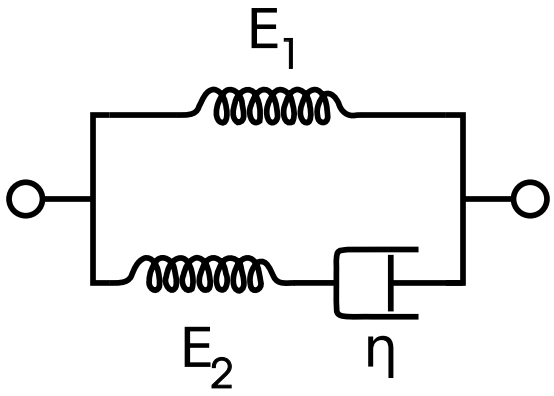

Figure 2.21: Standard Linear Solid model: a spring in parallel with a Maxwell branch [18]

To address the limitations of both the Maxwell and Kelvin–Voigt models, the Standard Linear Solid (SLS) model combines them: it places a spring in parallel with a Maxwell branch (i.e., a spring and damper in series). This structure allows the model to capture both creep and stress relaxation behaviors:

$$\dot{\varepsilon} = \frac{1}{\eta}(\sigma - E_1\varepsilon) + \frac{\dot{\sigma}}{E_2}$$

Where E_1 is the modulus of the parallel spring and E_2 is the modulus of the spring in the Maxwell branch.

This model offers a more accurate representation of viscoelastic materials compared to the simpler linear models. However, all of the above models remain linear and thus are limited in their ability to describe complex, nonlinear effects such as hysteresis, amplitude dependence, or rate-dependent stiffness, which are often observed in real bushing materials under large deformations or dynamic loading.

2.4.3 Tire modeling

Tire models play a critical role in the analysis and simulation of vehicle dynamics by representing the mechanical behavior of tires under different conditions. These models vary widely in complexity, ranging from basic empirical or analytical equations to advanced finite element (FE) simulations.

The choice of tire model is typically guided by the demands of the specific application. High-fidelity FE models are often used in tire design and development within the industry, as they can capture detailed structural behavior and material properties. However, their computational cost is significant, and they are generally too slow for integration with full vehicle dynamic models or for use in real-time simulations.

In contrast, multi-body tire models are designed to replicate the tire's overall physical response—such as force generation and deflection—without modeling its internal structure. These models offer a practical balance between accuracy and computational efficiency, making them suitable for vehicle system simulations and control development tasks where faster computation is necessary.

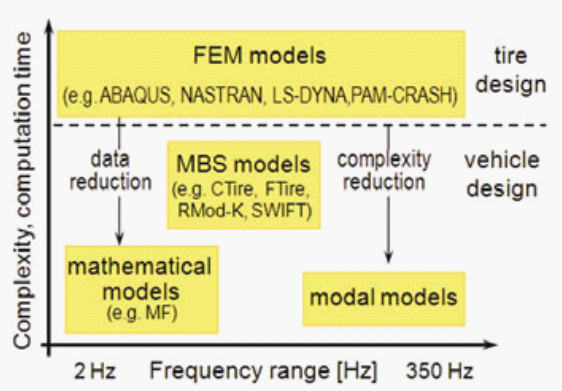

Figure 2.22: Representation of the different possible application ranges for various tire models [12]

2.4.3.1 Point contact tire model

The point contact tire model is a simplified mathematical approach commonly used to represent the interaction between a tire and the terrain. In this model, the contact between the tire and the ground is idealized as occurring at a single point, known as the ground-contact point. All tire forces and moments are assumed to act through this point, which is defined as the intersection of three geometric planes: the wheel plane, the ground plane, and a third plane passing through the wheel center that contains the normals of the other two. This model simplifies the tire-ground interface by assuming the terrain beneath the wheel can be approximated by a local tangent plane. However, this assumption limits the model's applicability to smooth, continuous surfaces. Specifically, it is valid only when there are no step changes in terrain elevation or slope, the wavelength of terrain undulations is at least three times the contact patch length, and the ground surface within the contact patch can be adequately approximated by a flat plane. While computationally efficient, the point contact model fails to capture the distributed nature of real tire-ground contact[20].

2.4.3.2 Radial spring tire model

The study conducted by [7] presented a radial spring tire modeling approach to characterize the tire–road interaction in the vertical plane. In this methodology, the tire is represented as a collection of radial spring-damper elements that are symmetrically distributed about the wheel centre. Each of these elements acts as a radial strut extending from the wheel hub to the tire surface, compressing when in contact with the road. The road is assumed to be rigid, and all deformation is considered to occur within the tire, specifically in the radial direction. Shear deformation along the circumference of the tire is neglected.

The contact force between the tire and the road arises from the radial deflection of these elements as the tire rolls and deforms against the ground. Only the elements within the contact patch—defined by the angular envelope of contact—contribute to the overall force. Each element generates a force proportional to its radial deflection and the relative vertical velocity, but only when the tire is in compression at that location.

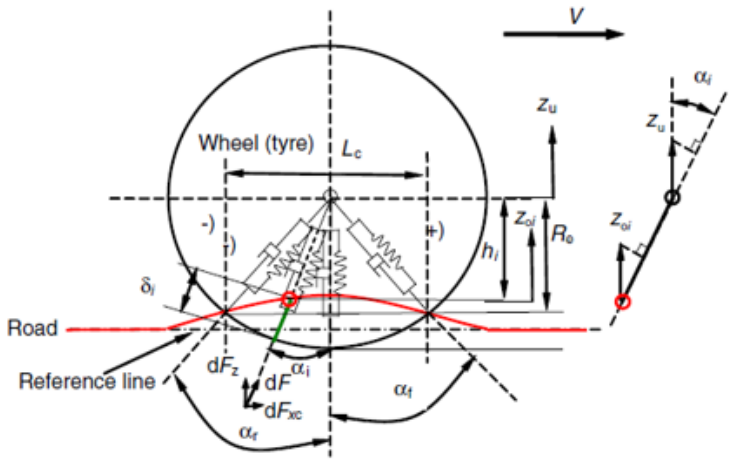

Figure 2.23: Radial-spring tire–ground contact model. [7]

The force contributed by each element is defined as:

$$dF = \begin{cases} (K_t \cdot \delta_i + C_t \cdot \dot{v}_i) \cdot d\alpha_i, & \text{if } \delta_i > 0 \\ 0, & \text{if } \delta_i \leq 0 \end{cases}$$

where:

- K_t is the spring stiffness per unit angle (N/m·rad),
- C_t is the damping coefficient per unit angle (Ns/m·rad),
- δ_i is the radial deflection at angular position α_i,
- $\dot{v}_i$ is the relative radial velocity at α_i,

- $d\alpha_i$ is the angular width of the element.

To compute the total contact forces, these elemental contributions are integrated over the active contact patch (bounded by front and rear angles α_f and α_r):

$$F_z = \int_{\alpha_r}^{\alpha_f} (K_t \cdot \delta_i + C_t \cdot \dot{v}_i) \cos(\alpha_i)\, d\alpha_i$$

$$F_{xc} = -\int_{\alpha_r}^{\alpha_f} (K_t \cdot \delta_i + C_t \cdot \dot{v}_i) \sin(\alpha_i)\, d\alpha_i$$

On a flat surface, the contact patch becomes symmetric ($\alpha_f = -\alpha_r = \alpha_t$), and the geometry simplifies. The vertical contact force and effective contact parameters can then be calculated using:

$$F_z = 2K_t R(\sin\alpha_t - \alpha_t \cos\alpha_t) - C_t \dot{z}_u(\cos\alpha_t \sin\alpha_t + \alpha_t)$$

$$F_{xc} = 0$$

where:

- R is the undeformed tire radius,
- $\dot{z}_u$ is the vertical velocity of the unsprung mass,
- α_t is the angular half-length of the contact patch, given by:

$$\alpha_t = \cos^{-1}\left(\frac{R - \delta_0}{R}\right), \quad \delta_0 = z_o - z_u$$

Additionally, the contact patch length and effective rolling radius are given by:

$$L_c = 2R\sin(\alpha_t), \quad R_e = R\cos(\alpha_t)$$

2.5 Rigs

2.5.1 K&C rig

Kinematics and Compliance (K&C) rigs are test machines used to measure how a vehicle's suspension and steering systems behave under controlled movement and loading. Typically, the vehicle body is rigidly clamped while each wheel is mounted on an independent plate that can move in multiple directions—vertically, laterally, and longitudinally.

The rig is equipped with high-precision sensors to measure displacements, rotations, and forces at key points such as the wheel center and contact patch. During kinematics testing, the suspension is cycled through its travel (e.g., by moving the plates

vertically or steering them) to observe how parameters such as camber, toe, caster, and track width evolve. This reveals the geometric characteristics of the suspension throughout its range of motion.

In compliance testing, known forces and moments are applied at the contact patch, and the resulting deflections are measured. This helps quantify how flexible the suspension structure is—i.e., its compliance—under different load paths. From these tests, various stiffness rates can be derived, including lateral, longitudinal, and aligning torque stiffness.

A specific type of K&C rig is the Suspension Parameter Measurement Machine (SPMM), which differs in its method of input application. Rather than moving the wheels while the vehicle body is fixed, the SPMM moves the vehicle body over a fixed ground plane, with the wheels remaining stationary.

Figure 2.24: SPMM rig [9]

2.5.2 Shaker rig

A shaker rig is a common laboratory test setup used to evaluate the vertical ride characteristics of a vehicle by simulating road-induced excitations. The system consists of four hydraulic actuators—one beneath each wheel—that can independently apply vertical motion to simulate road inputs while the vehicle remains stationary in a controlled environment.

The primary goal of shaker rig testing is to analyze how the vehicle's suspension and body respond to vertical displacements, enabling the study of primary ride behavior, vertical vibration modes, and component tuning such as springs and dampers. The actuators can replay real road profiles, apply sine sweeps, or execute standardized test sequences to represent different driving conditions.

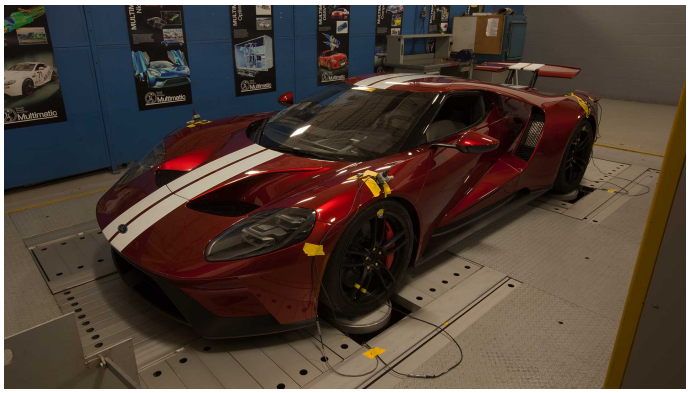

Figure 2.25: Shaker rig [10]

2.6 Transmissibility

Transmissibility is defined as the ratio of the output to the input. It tells us, for an input force, how much of it is passed through to the output. In vehicle testing setups such as a shaker rig, the system is subjected to sinusoidal inputs across a range of frequencies. As the frequency of the input changes, the system's response also varies. To analyze this behavior across different frequencies, transmissibility is expressed as a function of frequency. In such cases, it is treated as a complex-valued function referred to as the frequency response function (FRF).

This complex-valued transmissibility captures both the amplitude ratio (magnitude) and the phase difference between the input and output signals at each frequency. Such representation is especially useful when estimating transmissibility from measured time-domain signals, enabling engineers to understand key dynamic behaviors like resonant peaks (natural frequencies), phase shifts, and vibration isolation efficiency of the system. The frequency-dependent nature of transmissibility is what allows it to reflect how systems respond differently to inputs of varying frequencies.

The frequency response function $T(f)$ is mathematically expressed as [16]:

$$T(f) = \frac{G_{yx}(f)}{G_{xx}(f)}$$

Where:

- $T(f)$ is the transmissibility (complex-valued, frequency-dependent),
- $G_{yx}(f)$ is the cross power spectral density between the output signal $y(t)$ and the input signal $x(t)$,
- $G_{xx}(f)$ is the auto power spectral density (PSD) of the input signal $x(t)$.

2.7 Nonlinear least squares and curve fitting

Curve fitting is a fundamental task in engineering and science, where the objective is to determine parameters of a model so that its output closely replicates a set of observed data. When the relationship between the model and its parameters is nonlinear, the curve fitting problem becomes one of nonlinear least squares optimization.

As described by Dennis [19], nonlinear least squares aims to find the parameter vector $\mathbf{x} \in \mathbb{R}^n$ that minimizes the sum of the squares of residuals — the differences between observed data and model predictions. Mathematically, this is expressed as:

$$\min_{\mathbf{x}\in\mathbb{R}^n} \ \phi(\mathbf{x}) = \frac{1}{2}\sum_{i=1}^{m} [f_i(\mathbf{x}) - y_i]^2 = \frac{1}{2}\|\mathbf{r}(\mathbf{x})\|^2,$$

where $f_i(\mathbf{x})$ represents the model output for the i-th data point, and y_i is the corresponding measured value. The function $\mathbf{r}(\mathbf{x}) \in \mathbb{R}^m$ is the residual vector, and $\phi(\mathbf{x})$ is the objective function being minimized.

This formulation provides a systematic framework for curve fitting: the model is treated as a function of unknown parameters, and optimization techniques are used to adjust these parameters to reduce the discrepancy between predicted and observed data.

Dennis emphasizes that nonlinear least squares problems possess a unique structure that can be exploited by specialized iterative methods such as the Gauss–Newton and Levenberg–Marquardt algorithms. These methods use first-order derivative information — specifically, the Jacobian matrix of the residual vector — to approximate the curvature of the objective function. The Gauss–Newton method linearizes the residual function at each iteration and solves a sequence of linear least squares problems, assuming the residuals are small and nearly linear in the parameters. The Levenberg–Marquardt method modifies this approach by introducing a damping term, which blends the Gauss–Newton direction with a scaled gradient descent step, thereby enhancing robustness when the residuals are large or the model is highly nonlinear. Both methods exploit the fact that the objective function in least squares problems is a sum of squared terms, allowing for efficient and reliable parameter estimation when properly applied.

In the context of curve fitting, this approach is especially valuable for dynamical systems and models governed by differential equations, where model outputs cannot be expressed as simple functions of the parameters. By minimizing the residuals between simulated outputs and empirical data, nonlinear least squares serves as a powerful tool for identifying model parameters that yield accurate fits.

3

Methods

This chapter presents the methodologies utilized for modeling, data collection, and data analysis within the project. Testing was conducted on three vehicles, including rig and track measurements. Data gathered from the rig was used to quantify the model parameters, using optimization techniques to fit the parametrized model response to the measurements. Conversely, track-collected data was used to evaluate the complete model by simulating the real-life scenario. The quarter car model was implemented in a modular fashion to efficiently suit various vehicle axle architectures.

An overview of the project workflow is shown in Figure 3.1.

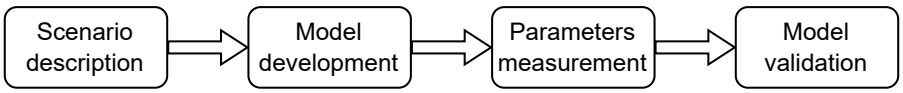

Figure 3.1: Methodology overview

3.1 Modeling complexity determination

The objective of the model in this study is not to deliver absolute predictions of vehicle performance (such as maximum ride comfort scores or precise acceleration transmissibility), but rather to explore how key suspension and body parameters influence ride behavior—particularly in the domains of *impact harshness*. As such, the model must strike a balance between **sufficient dynamic realism** and **computational efficiency**, enabling its use as an early-stage design tool.

To meet this objective, the following key requirements were defined:

- **Sensitivity over specificity**: The model must be sensitive to changes in suspension and body parameters in a manner that reflects real vehicle measures. It is not required to produce exact numerical outputs matching a specific vehicle, but rather to replicate *relative* behavior trends.
- **High-frequency relevance**: As explained in 2.1, the impact scenario is a combined motion hence, the model must capture vertical and longitudinal dynamics to a degree sufficient for analyzing high-frequency ride inputs, such as impacts.

- **Fast iteration and flexibility**: Since early development involves exploring a wide design space, the model must allow rapid parameter tuning and simulation execution, enabling it to support trade-off studies and performance target setting.

To support the above objectives and the requirements, a **quarter car** modeling approach was adopted as the pitching effects were determined to be negligible for the impact scenario. Given the scenario has dynamics in both vertical and longitudinal direction appropriate suspension modeling was considered along with a independent tyre model to handle the tyre interaction and decide the forces into each suspension model.

3.1.1 Vertical Suspension Modeling Approach

The vertical dynamics were captured using a model with up to five degrees of freedom (5-DOF), incorporating the standard sprung and unsprung masses, along with additional lumped masses representing the powertrain, subframe, and damper/-top mount assemblies. These components were included based on their relevance and dynamic participation at higher frequencies. Their inclusion ensures that the model can capture the dominant high-frequency modes critical for analyzing impact events.This modeling approach provides the necessary dynamic representation to support early design decisions, enabling efficient evaluation of suspension trade-offs and ride impact targets without the overhead of full vehicle simulations.

3.1.2 Longitudinal Suspension Modeling Approach

The dynamics in the longitudinal direction are captured using a model with up to six degrees of freedom (6-DOF), comprising both unsprung masses (representing each axle), a single sprung mass, a subframe, and up to two powertrain-related masses. These elements were selected based on the primary load path in the longitudinal direction and the dynamic behavior of components that significantly contribute to impact transmission. Their inclusion allows the model to reflect the coupled longitudinal response during cleat events and capture relevant dynamics associated with drivetrain compliance, subframe isolation, and axle-to-body interactions.

3.1.3 Tyre Modeling Approach

Two tire modeling approaches were adopted in this study to address different simulation needs. The first is a traditional point-contact model, which simplifies the tire as a single contact point with vertical stiffness. This model is suitable for vertical-only vibration analysis and was primarily used for parameter estimation through optimization against shake rig data. The second is a radial spring-damper-based contact model, which represents the tire as a radial element located at a single point on the circumference, incorporating both stiffness and damping. This approach is better suited for cleat impact evaluation, as it captures the necessary longitudinal compliance and localized contact behavior required to reflect the transient dynamics during tire-obstacle interaction.

The force elements in the above-described models have been simplified to linear spring-damper representations to satisfy the requirement for modeling simplicity. However, provisions for incorporating nonlinearities, particularly in the suspension components, have been considered in the model structure to allow for future refinement if needed.

3.2 Parametrization

The quarter car model is parameterized using aggregated or system-level parameters. This means that, instead of using component-level parameters such as damper rate or bushing stiffness, the effective value at the system is used, for example the wheel to body stiffness. Other examples are the powertrain (PWT) or the sub-frame (SF) stiffness, which is the combined stiffness from all their corresponding bushings, in either the vertical or the longitudinal direction. The system-level parameters are also the ones measured by the K&C rig.

To manage parameter values across the modeled vehicle axles, a database-inspired system was developed to organize and store all relevant parameter values in a structured and centralized format. This approach is especially important when handling multiple vehicle variants, as it ensures consistency in parameter definition, reduces errors, and simplifies integration into simulation models. A vehicle template was created in MATLAB including all parameters that may be used by the model. Each parameter entry includes the following information:

- **Name**: The name of the parameter.
- **Model variable**: The corresponding variable name used in the model.
- **Value**: The parameter baseline value.
- **Unit**: The physical unit (e.g., N/m, kg).
- **Range**: The valid range for the parameter estimation process, explained in Section 3.5.
- **Comment**: Additional notes.

Table 3.1 presents the list of parameters used in the model. For each vehicle modeled, the template includes parameter sets for both the front and rear axles, which results in a combined front and rear parameter table for the vehicle. Note that the parameters are corner-level, even though the model represents an axle.

A naming convention was established to generate concise and consistent variable identifiers for use in the model. Each DoF was initially named as wheel, body, top mount (TM), sub-frame (SF) and powertrain (PWT) and the general physical quantities were assigned the following prefixes: mass as `m`, stiffness as `k`, and damping as `c`. Each parameter name is constructed according to the following pattern: `name = [type]_[component]_[axis]`.

If the component is only present in a single direction (e.g., vertical), the axis suffix

may be omitted. For instance, the stiffness of the top mount is defined as `k_TM`, while the vertical stiffness of the subframe is written as `k_SF_Z`.

	Parameter	**Identifier**	**Description**
Masses	Total mass		Total vehicle mass
	Mass distribution F2R		Front to rear vehicle weight distribution
	Unsprung mass	`m_wheel`	Corner unsprung mass, also referred as wheel mass in this work.
	Top mount (TM) mass	`m_TM`	Mass representing the damper body and top mount bushing
	Sub-frame (SF) mass	`m_SF`	Equivalent corner mass of the axle's SF (0.5 times the total)
	Powertrain (PWT) mass	`m_PWT`	Equivalent corner mass of the axle's PWT (0.5 times the total). Contains the motor and transmission, and any other rigidly-attached bodies
Vertical	Wheel to body stiffness	`k_wheel_Z`	Equivalent vertical stiffness between wheel and body
	Wheel to body damping	`c_wheel_Z`	Equivalent vertical damping between wheel and body
	TM stiffness	`k_TM`	Stiffness between TM and body
	TM damping	`c_TM`	Damping between TM and body
	SF stiffness	`k_SF_Z`	Equivalent vertical stiffness between SF and body
	SF damping	`c_SF_Z`	Equivalent vertical damping between SF and body
	PWT stiffness	`k_PWT_Z`	Equivalent vertical stiffness between PWT and body, or PWT and SF
	PWT damping	`c_PWT_Z`	Equivalent vertical damping between PWT and body, or PWT and SF
	Spring Motion Ratio	`MR_susp_spring`	Motion ratio used to compute the reaction force at the SF
	Damper Motion Ratio	`MR_susp_damper`	Motion ratio used to compute the reaction force at the SF

	Parameter	Code	Description
Longitudinal	Wheel to body stiffness	`k_wheel_X`	Equivalent longitudinal stiffness between wheel and body
	Wheel to body damping	`c_wheel_X`	Equivalent longitudinal damping between wheel and body
	SF stiffness	`k_SF_X`	Equivalent longitudinal stiffness between SF and body
	SF damping	`c_SF_X`	Equivalent longitudinal damping between SF and body
	PWT stiffness	`k_PWT_X`	Equivalent longitudinal stiffness between PWT and body, or PWT and SF
	PWT damping	`c_PWT_X`	Equivalent longitudinal damping between PWT and body, or PWT and SF
Tire	Tire stiffness	`k_tire`	Tire vertical stiffness over a flat surface
	Tire damping	`c_tire`	Tire vertical damping over a flat surface
	Tire unloaded radius	`R_tire`	Nominal unloaded radius of the tire
	Tire static load	`static_ tire_load`	Static vehicle weight on the corresponding corner
	Tire static deflection	`static_ tire_def`	Vertical tire deflection under static load

Table 3.1: Axle model parameters grouped by sub-model, with associated identifiers and descriptions.

3.3 Modeling

The modeling approach consists of two main steps: vehicle suspension modeling and tire modeling. The suspension model is further divided into two independent sub-models, one in the vertical (z) direction and the other in the longitudinal (x) direction. Each computes the vehicle's dynamic response from the wheel center upward. This results in three distinct model blocks, as shown in Figure 3.2.

The role of the tire model is to calculate the forces at the wheel center—both in the x and z directions—arising from the interaction between the tire and the road surface. These forces serve as input signals to the corresponding suspension sub-models.

This modular structure provides a clear separation between tire-road interaction and suspension dynamics. It offers flexibility to independently modify or replace components—such as testing alternative tire models—without affecting the rest of the system.

The complete model is implemented as a MATLAB function compatible with MATLAB's built-in ODE solvers. The function integrates the three modules of the model and manages their interconnection according to the structure illustrated in Figure 3.2.

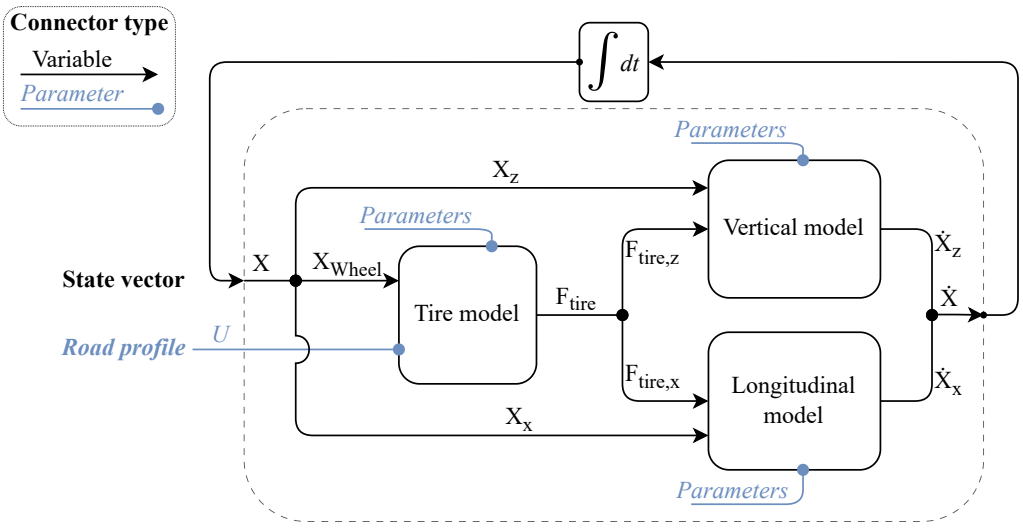

Figure 3.2: Complete model diagram

The variables illustrated in Figure 3.2 are defined as follows:

- $\boldsymbol{X}$: State vector containing the instantaneous positions and velocities of all masses in the model, in both the longitudinal (x) and vertical (z) directions.
- $\boldsymbol{X}_{\text{Wheel}}$: Position and velocity of the wheel center, in both the longitudinal (x) and vertical (z) directions.
- $\boldsymbol{U}$: Model input vector, consisting in the complete road profile.
- $\boldsymbol{F}_{\text{tire}}$: Force vector computed by the Tire model, applied to the wheel center.
- $\dot{\boldsymbol{X}}$: State derivative vector

3.3.1 Vehicle suspension model

The components of the model are categorized into two types: mass elements and force elements. Mass elements represent isolated inertial components, which generally are large elements such as the body or the powertrain (PWT). Force elements correspond to elastic and damping components—such as bushings, spring and dampers—that interconnect the masses. Each force element generates a force based on the relative displacement between the masses it connects. The same modeling approach is applied in the longitudinal direction, with the primary difference being the absence of gravitational acceleration.

3.3.1.1 Model schematic and equations

Figure 3.3 illustrates the steps involved in developing the model. The first step is to create a schematic representation of the masses and the force elements that connect them. It is important to clearly visualize the relative positions of the masses, identifying which masses are positioned above or below one another and the corresponding force elements located between them. The subsequent step consists of defining the equations that describe the forces generated within the system, as well as the accelerations of each mass resulting from these applied forces.

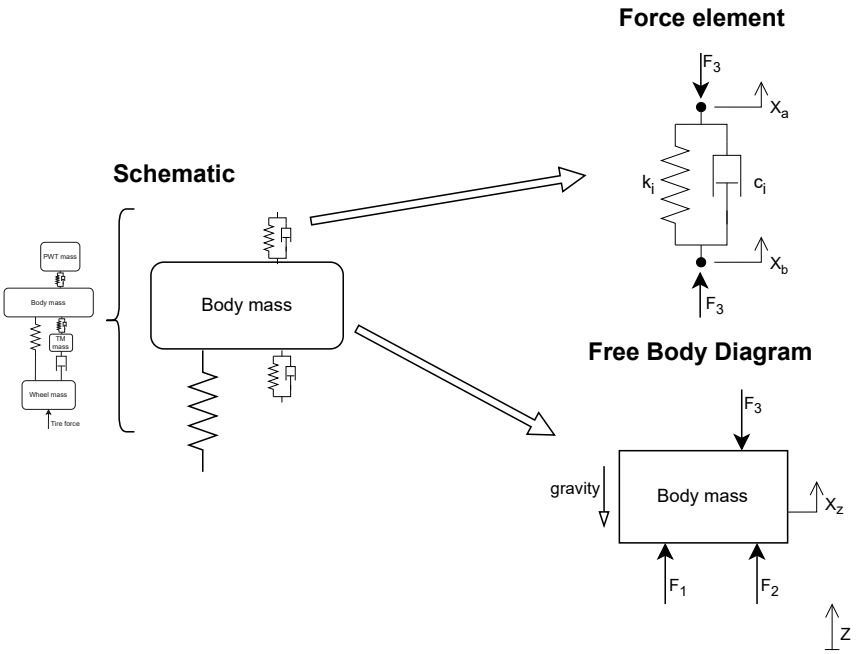

Figure 3.3: Modeling process, focused on one of the masses in the model.

A sign convention was established for displacement and force definitions, as reflected in Equation 3.1 and 3.2. Specifically, a force element generates a positive force when it acts outward—i.e., it "pushes" to pull the connected masses apart. Correspondingly, the displacement—representing how much the spring is stretched—is positive when the spring is extended relative to the initial position.

The relative displacement and velocity between two connected masses, exemplified in the vertical direction, are defined as:

$$\Delta X_i = X_{a,z} - X_{b,z}, \quad \Delta \dot{X}_i = \dot{X}_{a,z} - \dot{X}_{b,z} \tag{3.1}$$

The resulting spring and damper forces are then expressed as:

$$F_{\text{spring,i}} = -k_i \, \Delta X_i, \quad F_{\text{damper,i}} = -c_i \, \Delta \dot{X}_i \tag{3.2}$$

where:

- $X_{a,z}$ and $X_{b,z}$ are the positions of the two connected masses in z direction,
- $\dot{X}_{a,z}$ and $\dot{X}_{b,z}$ are the corresponding velocities,
- ΔX_i and $\Delta \dot{X}_i$ are the relative displacement and velocity,
- k_i and c_i are the spring stiffness and damping coefficient,
- $F_{\text{spring},i}$ and $F_{\text{damper},i}$ are the corresponding spring and damper forces.

The dynamics of each mass is driven by its acceleration, which is calculated according to the equation obtained by deriving the corresponding free-body diagram (FBD), as exemplified in Figure 3.3. The Equation 3.3 is the generalized acceleration equation of each mass.

$$\ddot{X}_n = -g + \frac{1}{m_n} \sum_i F_i \tag{3.3}$$

where:

- $\ddot{X}_n$ is the acceleration of the n-th mass,
- m_n is the n-th mass value,
- F_i represents the i-th force acting on the n-th mass,
- $\sum_i$ denotes summation over all forces acting on the n-th mass.

3.3.1.2 Suspension model implementation in MATLAB

The generation of model equations is performed in a modular and automated manner using the MATLAB Symbolic Toolbox. This approach enables the creation of different model variants, which are adapted to different axle architectures, and produces fully parameterized equations that allow the model to be evaluated across different vehicle parameters.

The vertical implementation of the model also incorporates the point-contact tire model, which is described in Section 3.3.2.1 and consists of an additional spring–damper element placed between the road input and the wheel mass. Additionally, two more inputs are present: gravitational acceleration and an external wheel center force, the latter being used by the radial tire model described in Section 3.3.2.2. As a result, the vertical suspension model requires a total of four inputs: road height, road velocity, wheel center force and gravitational acceleration. In contrast, the longitudinal model is driven by only the wheel center longitudinal force.

The process of generating the equations begins with defining a model configuration, which governs how the equations are assembled. The configuration specifies:

- **Mass deactivation:** The top mount (TM), powertrain (PWT), and subframe (SF) mass dynamics can be excluded from the model.

- **Suspension spring and damper layout:** These may act directly on the upright (e.g., McPherson strut configuration) or through a suspension arm with an associated motion ratio.
- **PWT position:** The PWT mass may be suspended either on the sub-frame or directly on the vehicle body.
- **Suspension reaction position:** Both spring and damper forces can be reacted individually either directly on the body (the more common scenario) or on the sub-frame.

Based on the specified configuration, the equation generation algorithm first formulates the individual force equations for each force element, then integrates them into the mass acceleration equations. When a mass is deactivated, the corresponding equation remains present but is evaluated as zero. This design choice maintains a consistent acceleration vector length across configurations, which results in the later generated system matrices having a uniform size regardless of the model variant.

Once the equations are assembled, the state-space representation is generated automatically by computing the corresponding Jacobian matrices of the differential equations, which forms the linear State Space system matrices.

The resulting model is provided as a MATLAB function that returns the system matrices evaluated with the parameter values. This functional format allows its use as a grey-box model within MATLAB's System Identification Toolbox.

The two figures below show the suspension schematics for a one particular axle configuration. The system is modeled with 5 degrees of freedom, employing a McPherson strut layout, and includes the powertrain mounted directly on the vehicle body.

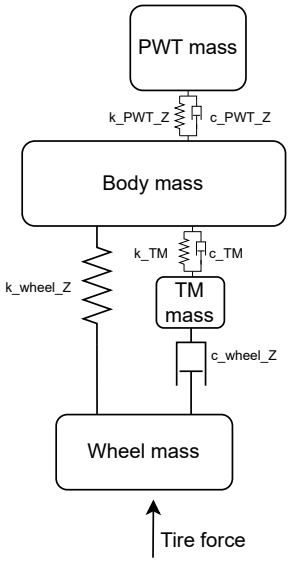

Figure 3.4: Vertical model schematic.

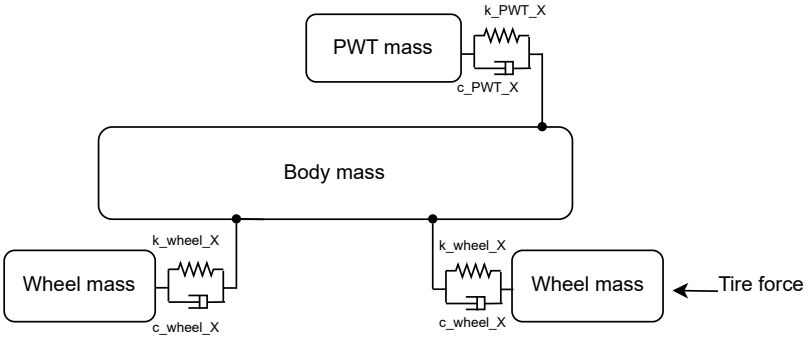

Figure 3.5: Longitudinal model schematic

3.3.2 Tire model

Both point-contact and radial spring tire models presented in Section 2.4.3 have been used in different scenarios. The point-contact model, which is limited to capturing vertical dynamics, has only been used in combination with the vertical suspension model, mainly for parameter estimation as described in Section 3.5). In contrast, the radial spring tire generates both vertical and longitudinal forces, making it suitable for use in the complete model.

3.3.2.1 Point contact model

The point-contact tire model consists of a simple vertical spring-damper element, representing the most straightforward modeling approach. It generates force exclusively along the vertical (Z) axis, as defined by Equation 3.2, which also applies to any linear force element within the suspension model.

Since the point-contact tire model is limited to use within the vertical suspension model, it has been directly integrated into the vertical suspension model equations, as an additional force element.

3.3.2.2 Radial spring tire model

The key feature of the radial spring tire model is its ability to capture the interaction with a non-planar road input. It determines the direction of the total force applied at the wheel center, from which the longitudinal and vertical components are computed to serve as inputs to the combined suspension model.

Rather than using discrete spring elements distributed around the tire circumference, a different approach is adopted: the intersected area between the tire's unloaded circular profile and the road profile is computed. The magnitude of the force generated depends on the total contact area, while its direction is given by the vector from the centroid of the contact area to the tire center, as illustrated in Figure 3.6.

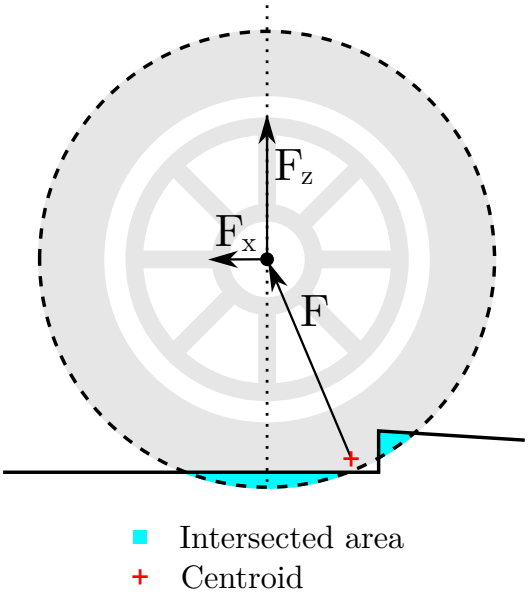

Figure 3.6: Tire model principle represented over a cleat.

Damping forces arise from the velocity of the contact area, defined as the change in contact area divided by the time interval between two samples. This area change is split into positive (compression) and negative (rebound) increment, each associated with its own centroid and resultant force direction. Differentiating between compression and rebound is essential to isolate and limit rebound damping forces, ensuring they do not exceed the spring force. This limitation prevents the resultant

force from unrealistically pulling the tire downward onto the ground. Figure 3.7 illustrates the area increment for a certain wheel center velocity direction.

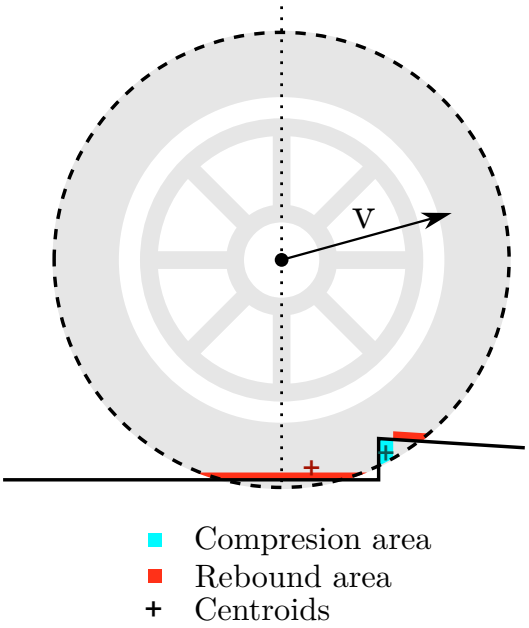

Figure 3.7: Tire model damping force principle.

To parametrize the tire model, the following requirements were established:

1. Static load and deflection point, determined from the vehicle measurements. This ensures that the model replicates the same geometric scenario observed in the real vehicle test.
2. Tire stiffness and damping rates at the static deflection point. These parameters are defined through the parameter estimation process and will govern the tire's dynamic response around the static deflection position.

These constraints are used to fit a spline curve that defines a reasonable tire force response as a function of planar contact patch deflection, as illustrated in Figure 3.8.

However, since the model evaluates the contact area instead of the radial deflection, the same force response must be reformulated as a function of the equivalent contact area. This area is computed using Equation 3.4, which geometrically defines the circular segment area as a function of deflection. The resultant force response with respect to contact area is shown in Figure 3.9. This target force response is ultimately achieved by evaluating a fitted polynomial function that approximates the desired force–area curve for a given contact area.

$$A(def) = R^2 \cdot \cos^{-1}\left(\frac{R - def}{R}\right) - (R - def) \cdot \sqrt{2 \cdot R \cdot def - def^2} \tag{3.4}$$

Where:

- A — Contact area (m^2)
- R — Tire radius (m)
- def — Vertical deflection of the tire (m)

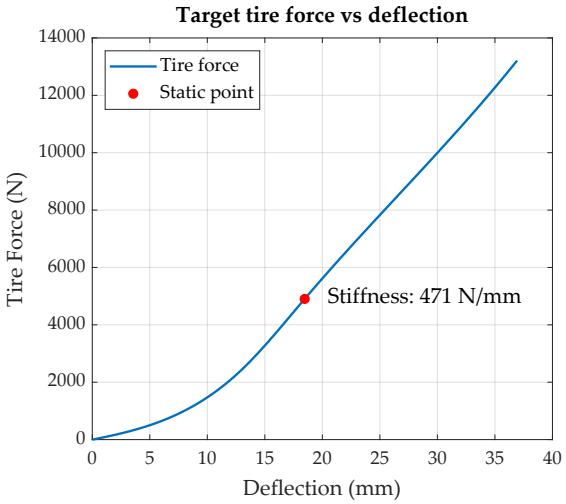

Figure 3.8: Example of a tire force response as a function of planar deflection (target stiffness: 450 N/mm).

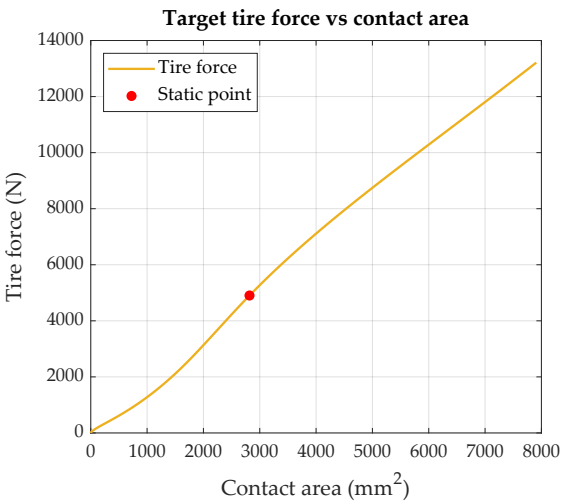

Figure 3.9: Example of a tire force response as a function of contact area.

To achieve the desired damping rate at the static deflection point, the area–deflection relationship from Equation 3.4 is differentiated to obtain the ratio between deflection velocity and area velocity. This ratio, evaluated at the static deflection point, is then used to scale the damping rate from deflection-based to area-based velocity.

3.4 Measurements

Three vehicles have been measured during two campaigns, including a variety of platforms, with different suspension layouts and powertrain architectures. The first campaign learning was applied to improve the data collected during the second one.

The relevant data captured for the project included, on one hand, the stiffness of the vehicle's suspension elastic elements—such as springs and bushings—which were directly measured using the K&C rig. On the other hand, the dynamic response was recorded using the Shaker rig by measuring the acceleration of vehicle components that are also represented in the model, such as the powertrain.

3.4.1 4-Post Shaker rig measurements

The test involves a single-axle excitation, applying a sinusoidal signal that sweeps frequency from 0.5 Hz to 30 Hz. The signal magnitude is defined by the peak velocity of the signal, which is maintained at a constant value during each run, with multiple runs conducted at different peak velocities ranging from 5 mm/s to 150 mm/s. The

range of magnitudes tested can reveal the amplitude dependence of the suspension response, which can be used to evaluate the non-nonlinearities of the system.

The sensor setup includes accelerometers placed at the wheel and the vehicle body, with additional channels at the powertrain and sub-frame, if present in the measured vehicle. These extra sensors aim to capture the resonance of the masses suspended on the vehicle body, which are also present in the model, depending on the axle architecture of the measured vehicle. Additional channels were also used at various points of the powertrain to identify rotational oscillations. All signals were recorded at a sampling frequency of 1 kHz.

3.4.2 K&C rig measurements

The Suspension Parameter Measuring Machine (SPMM) K&C rig was used to measure both vertical and longitudinal suspension characteristics, with a primary focus on evaluating the stiffness of the wheel and sub-frame suspensions. The sensor setup consists of position tracking of the wheel center, which is integrated into the rig, along with a camera-based tracking system that monitors the position of the vehicle sub-frame. The rig also records all the forces applied at the contact patch. This configuration enables the calculation of sub-frame suspension stiffness when suspension loads are reacted on it.

Table 3.2 details the individual tests performed, which provided the data used to calculate the suspension parameters discussed in Section 3.4.4.1.

Test	Description	Velocity	Amplitude
Bounce	Vertical cycle, complete travel	quasi-static	suspension travel
Dynamic Bounce	Vertical sinusoidal cycle at several peak vel.	25 - 125 mm/s	±20 mm
Longitudinal	Longitudinal cycle, limited by force	quasi-static	±3500 N

Table 3.2: Performed tests in the K&C rig

3.4.3 Track cleat test measurements

An extension of the regular impact harshness (IH) test was defined to collect a wide range of data that characterizes the vehicle response to later compare with the model. It consist of running over several cleats of different sizes at a constant velocity. Different runs at different velocities were performed as well. The conditions are specified in the Table 3.3.

The sensor setup is similar to the one used in the Shaker rig measurements, consisting of accelerometers placed at each one of the masses present in the model, which includes wheel upright, vehicle body, powertrain and sub-frame. In contrast with

the Shaker rig, two sensors are used in each position to measure the acceleration in both Z and X axis.

Run	Velocity (Km/h)	Cleat height (mm)
1	20	10, 20, 30, 40
2	30	10, 20, 30, 40
3	40	10, 20, 30, 40

Table 3.3: IH test conditions

3.4.4 Data post-processing

The data collected from the rigs was post-processed in both time and frequency domains. For the IH tests, the measured signals were used directly to compare with the model's response, with minimal pre-processing to organize the test runs for efficient comparison and analysis.

3.4.4.1 Measured parameters

Wheel stiffness and damping, in both the vertical and longitudinal directions, were initially extracted directly from the time-domain data obtained with the K&C rig. These parameters values are representative at static or low-speed conditions, and may differ significantly from effective values observed at higher frequencies. They were primarily calculated by evaluating the gradients of force–displacement and force–velocity curves.

Friction in the suspension was also estimated from the test data. Although it is not included in the current model, it represents a potentially important nonlinear effect that could be incorporated in future iterations.

3.4.4.2 Transmissibility analysis

Transmissibility analysis was performed using the data from the SR10 rig. This method involves calculating the PSD of both an input and an output signal, and then computing the ratio of these PSDs across frequencies. The input in this case is the vertical acceleration measured at the shake rig's pad, while the output corresponds to each of the acceleration channels measured on the vehicle (e.g., wheel hub, powertrain, body).

In addition to calculating transmissibility from the shake pad to each channel, we also compute it between channels—for example, from the wheel to the body or from the body to the powertrain. This transmissibility typically corresponds to a specific spring-damper element in the model, which may represent either a bushing or an actual spring and damper from the vehicle.

The result represents the output response per unit input magnitude. In other words, it assumes a constant input acceleration amplitude (normalized to 1) and illustrates

how that input is transmitted through the system. However, because vehicle suspensions are inherently nonlinear, the resulting transmissibility curve is only valid as a ratio applied by the system in the recorded data conditions. At different excitation levels, the system may exhibit different gains due to the nonlinearities. Despite this limitation, transmissibility remains useful for the parameter fitting process described in Section 3.5, particularly since the model is a linear approximation of the real system.

3.4.4.2.1 Symmetry-based averaging

To improve robustness and reduce the influence of asymmetries or sensor noise, we also compute average transmissibility curves between symmetric components. For example, the left and right wheel hub transmissibilities (relative to the shake rig pad) are averaged to obtain a representative "pad-to-wheel" transmissibility. This is similarly done for other symmetric channels such as the body or subframe.

The averaging process is performed in the frequency domain by taking the pointwise mean of the transmissibility magnitudes from the left and right channels. This approach assumes that the system is approximately symmetric and that any deviations are due to measurement noise or minor structural differences. The averaged transmissibility provides a cleaner signal for model fitting and better represents the overall system behavior.

To further reduce the influence of pad imbalance, a virtual center pad is defined as the mean of the left and right pad signals. All transmissibilities are then recalculated relative to this virtual center, ensuring a more balanced reference point for the analysis.

3.5 Model parameter estimation

One of the goals of this thesis was to parameterize a vehicle model using measurement data. To achieve this, an optimization-based parameter estimation (Section 2.7) approach was employed. Two methods were explored for this purpose:

1. Grey-box model parameter estimation from MATLAB's System Identification Toolbox
2. A custom optimization using a user-defined cost function

The **custom optimization** method described in Section 3.5.2 was chosen as the best fit for our application.

This estimation was performed in the frequency domain, which provides a suitable framework for comparing the harmonic response characteristics of the model and the physical system. The time domain frequency response data acquired through a 4-post shake rig (refer that measurement section) were converted to frequency domain (refer transmissiblity analysis section).

The following sections describe the two approaches used for parameter estimation in more detail.

3.5.1 Grey-box parameter estimation using system identification toolbox

Model parameter estimation was carried out using MATLAB's `greyest()` function, an off-the-shelf tool provided by the System Identification Toolbox. This function is specifically designed for estimating parameters of grey-box models using recorded data. Using `greyest()` requires adhering to the syntax and workflow defined by the toolbox, including the use of associated functions such as `idgrey`, `iddata`, and `setpar`. In addition to its estimation facility, the toolbox offers effective handling of measurement data and includes built-in visualization tools that help evaluate how well the model fits the data throughout the estimation process.

To perform the estimation, the parametric state-space quarter-car model was passed to `idgrey` to define the grey-box structure. The recorded measurement data were formatted using `iddata()`, and these two inputs were then provided to `greyest()` to estimate the parameters. Parameters of interest for estimation/fitting were selected for calibration using the `setpar()` function. Finally, `idplot()` was used to visualize the fit between the simulated model response and the experimental data.

Despite its convenience of being off the shelf tool, this approach has some notable limitations in the context of this study:

- The cost function used by `greyest()` is predefined and does not allow for custom formulations.
- There is limited flexibility to create custom weighting filters
- The estimation is constrained to direct input-output relationships, such as transmissibility from ground to a measured mass. This prevents fitting of inter-mass transmissibilities—such as wheel-to-body or powertrain-to-body—which were important in this study.

Although these drawbacks made using this method less suitable for the final implementation as estimation tool, it served as a useful reference during the development of the custom optimization approach described in the next section.

3.5.2 Custom optimization-based parameter estimation

To estimate the vehicle parameters, the custom parameter estimation aims to calibrate the parameters of the quarter car model such as (powertrain mass,topmount mass,stiffness, damping etc..) so that the dynamic response of the model closely matches the response recorded from the shake rig measurements. This is done by simulating the model's frequency response under the same test inputs and minimizing the mismatch/error between measured and simulated transmissibility, both in magnitude and phase. A cost function quantifying this mismatch/error is minimized using a nonlinear least squares solver

3.5.2.1 Cost function design

The optimization is based on comparing transmissibility functions between the model and measured data. However, not all possible transmissibility paths in the model are considered. Only channels that represent motion across a physical force element (e.g., tire, bushing, damper) and have corresponding measurements from the shake rig are included. For example, transmissibility at the top mount is excluded as it is not directly measured. For each selected channel and frequency, the cost function evaluates both the magnitude and phase errors between the measured transmissibility

$$e_{\text{mag}}^{(i,c)} = w_c(f_i) \cdot \frac{\lambda_c}{\text{scale}_{\text{mag}}} \cdot \left| 20 \cdot \left(\log_{10} \left| T_{\text{model}}^{(i,c)} \right| - \log_{10} \left| T_{\text{meas}}^{(i,c)} \right| \right) \right|$$

$$e_{\text{phase}}^{(i,c)} = w_c(f_i) \cdot \frac{1 - \lambda_c}{\pi} \cdot \left(\angle T_{\text{model}}^{(i,c)} - \angle T_{\text{meas}}^{(i,c)} \right)$$

where:

- λ_c is a channel-specific weighting factor that weights magnitude versus phase error.
- $\text{scale}_{\text{mag}}$ is a normalization factor(3dB) used to scale the magnitude error contribution.
- $w_c(f_i)$ is the frequency-dependent weight for channel c at frequency f_i
- $\log_{10} \left| T_{\text{model}}^{(i,c)} \right|$ and $\log_{10} \left| T_{\text{meas}}^{(i,c)} \right|$ are the magnitudes of the model and measured transmissibility, expressed in decibels.
- $\angle T_{\text{model}}^{(i,c)}$ and $\angle T_{\text{meas}}^{(i,c)}$ are the phase angles of the model and measured transmissibility.
- Phase values are unwrapped to avoid discontinuities and allow smooth comparison.

The full cost vector across all frequencies and channels is given by:

$$\mathbf{e} = \begin{bmatrix} e_{\text{mag}}^{(1,1)} \\ \vdots \\ e_{\text{mag}}^{(N,C)} \\ e_{\text{phase}}^{(1,1)} \\ \vdots \\ e_{\text{phase}}^{(N,C)} \end{bmatrix} \quad \text{with the objective function:} \quad J(\theta) = \|\mathbf{e}(\theta)\|^2$$

3.5.2.2 Frequency-selective weighting

To focus the fitting process on the most relevant dynamic bands, each transmissibility channel is assigned:

- a frequency band of interest (e.g., [0–3] Hz, [8–30] Hz),
- a scalar importance factor (e.g., 1.0, 0.75).

The frequency-dependent weight function is defined as:

$$w_c(f) = \begin{cases} \text{importance factor} & \text{if } f \in \text{band}_c \\ 0.05 \cdot \text{importance factor} & \text{otherwise} \end{cases}$$

This ensures that the optimizer prioritizes accuracy in the chosen frequency bands, while still penalizing large deviations outside those regions with a small baseline weight.

3.5.2.3 Optimization procedure

The parameter estimation process is performed using MATLAB's `lsqnonlin`, which solves a bounded nonlinear least squares problem. The optimization workflow is tailored to the vehicle's configuration and available test data, and proceeds through the following steps:

1. **Transmissibility Channel Selection**: Based on the model structure and axle configuration, only transmissibility paths that are physically meaningful and supported by available measurements are selected. This ensures that the selected channels reflect actual force transmission paths and that both input and output signals are recorded. Engineering judgment guides this selection.
2. **Initial Parameter Setup**: Physical parameters such as masses, spring rates, and damping coefficients are initialized using a combination of results from measurements (K&C), literature values, and practical engineering estimates. Only those parameters marked as "free to fit" are allowed to vary during optimization.
3. **Frequency Band and Channel Weighting**: Each transmissibility channel is assigned a frequency range of interest—typically targeting key dynamics like suspension resonances—and a scalar importance factor. These are used to construct frequency-dependent weights that emphasize fitting within critical bands while softly penalizing errors outside them.
4. **Cost Function Evaluation**: For each iteration, the model is simulated with the current parameter set to compute predicted transmissibility. The magnitude and phase errors between simulated and measured transmissibility are calculated across all selected frequencies and channels. These errors are scaled using the frequency- and channel-specific weights, and a tunable parameter that balances the relative importance of magnitude versus phase.
5. **Optimization**: The `lsqnonlin` solver updates the free parameters iteratively to minimize the total weighted error vector. All updates are bounded within physically plausible limits, ensuring realistic parameter values. The output is a set of tuned parameters that best match the dynamic behavior observed in the experimental data.

This process results in an optimal set of system parameters that closely replicate the measured transmissibility behavior within the relevant frequency bands.

3.5.2.4 Fit quality metric

To assess the quality of the model fit after optimization, a percentage-based fit metric is computed for each transmissibility channel's magnitude and phase. This metric maps the weighted error between model and measured responses into an intuitive fit percentage, with 100% representing a perfect fit.

For channel c, the magnitude fit percentage is defined as:

$$\mathrm{Fit}_{\mathrm{mag}}^{(c)} = 100 \times \exp\left(-k_{\mathrm{mag}} \cdot E_{\mathrm{mag}}^{(c)}\right)$$

where the weighted magnitude error is

$$E_{\mathrm{mag}}^{(c)} = \sum_i w_i \left| 20 \cdot \left(\log_{10} \left| T_{\mathrm{model}}^{(c)}(f_i) \right| - \log_{10} \left| T_{\mathrm{meas}}^{(c)}(f_i) \right| \right) \right|$$

Similarly, the phase fit percentage is

$$\mathrm{Fit}_{\mathrm{phase}}^{(c)} = 100 \times \exp\left(-k_{\mathrm{phase}} \cdot E_{\mathrm{phase}}^{(c)}\right)$$

where the weighted phase error is

$$E_{\mathrm{phase}}^{(c)} = \sqrt{\sum_i w_i \left(\angle T_{\mathrm{model}}^{(c)}(f_i) - \angle T_{\mathrm{meas}}^{(c)}(f_i) \right)^2}$$

Here,

- f_i are the frequency points,
- w_i are the normalized log-frequency weights such that $\sum_i w_i = 1$,
- k_{mag} and k_{phase} are decay constants controlling the sensitivity of fit to error,
- $|T|$ denotes magnitude and $\angle T$ denotes unwrapped phase.

The weights w_i compensate for the non-uniform spacing of frequency points on the logarithmic scale. They ensure that each frequency band contributes proportionally to the overall error by reflecting its relative width in log-frequency. This prevents bias toward densely sampled regions and provides a balanced fit metric across the spectrum.

3.6 Model simulation and evaluation

3.6.1 Simulation setup

Two different approaches were developed to simulate the model:

- **Linear state-space model simulation:** MATLAB's `sim()` function from the System Identification toolbox was used to compute the frequency response of a frequency-domain input data. This setup is limited to the suspension vertical model using the integrated point contact tire, and was therefore used exclusively during the parameter estimation process described in Section 3.5.
- **ODE model solver:** MATLAB's `ode45()` solver was employed to simulate the time-domain response of the complete model using a road profile as input.

The gravitational acceleration input is only required during the complete model simulation, primarily to ensure that the tire model is subjected to the correct normal load. In contrast, the parameter estimation process performs the simulation with zero gravitational acceleration, since the dynamics of the linear model are unaffected by constant forces such as gravity.

For the simulation of the complete model, a road profile representing the cleat input is provided. It consists of a vector of road samples, containing the road height and slope values at discrete longitudinal positions. The road profile begins with a flat section, followed by a vertical step of predefined height, a sloped descent, and a smooth transition back to the flat baseline using a continuous-curvature connection. As previously illustrated in Figure 3.2, the tire model samples the road profile according to the current wheel position, which is primarily determined by the vehicle's position.

3.6.2 Model evaluation procedure

All cleat test cases were simulated in an automated fashion, generating time-domain responses for each test condition according to the the cleat height and velocity combinations described in Section 3.4.3. This ensured a consistent model response for every measurement case and enabled large-scale evaluation of the model behavior.

Two error metrics were defined to assess model accuracy against experimental data. The first is the relative peak acceleration error, which quantifies the difference between the simulated and measured peak acceleration of the body mass (although it can be applied to other masses). The second is the RMS acceleration error during the after-shake period, capturing the discrepancy of the energy content during the decay phase after the cleat impact.

Both signals had to be temporally aligned to ensure consistency, which was achieved using the time of peak wheel vertical acceleration as a reference. The error metrics were then computed across the dataset, and then visualized using a histogram, as shown in the Results Section 4.4.2.

3.6.3 Model analysis variants

To isolate and analyze the influence of the tire model and the longitudinal suspension dynamics on the overall vertical suspension response—particularly the body vertical acceleration—two additional variations of the complete model were defined:

- **Longitudinally-locked model:** The longitudinal suspension model is excluded. As a result, the longitudinal velocities of the body, wheel and other masses is constant. This configuration reduces the system to a vertical suspension model coupled with the radial spring tire model.
- **Pure vertical model:** Both the tire model and the longitudinal dynamics are excluded, remaining only the vertical suspension model and the point contact tire. This model variant serves as a reference case to assess the dynamic contribution of the radial spring tire model to the system response.

4

Results

4.1 Sub-frame modal behavior analysis

The rear axles of all three tested vehicles have an isolated sub-frame, which supports the electric powertrain (PWT) and the suspension control arms. Each sub-frame was equipped with two accelerometers mounted at its front and rear end, to enable a vibrational analysis.

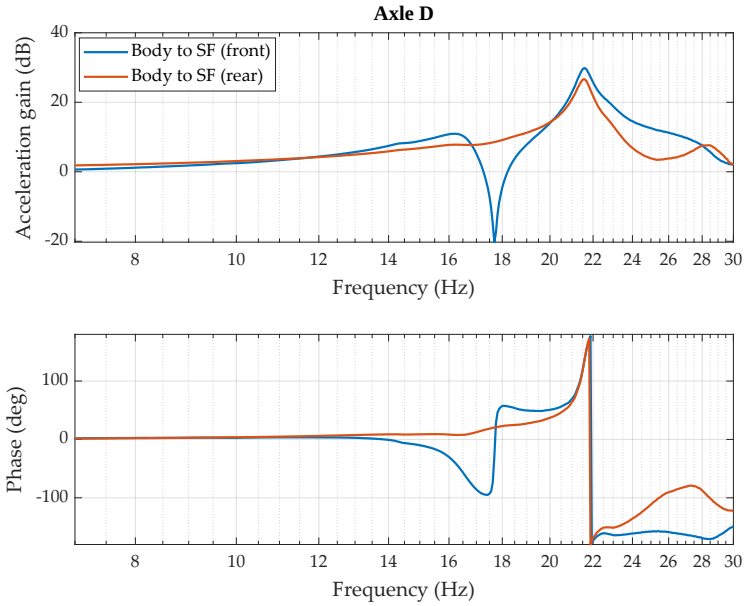

Figure 4.1: Measured transmissibility from body to front and rear end of the rear axle sub-frame.

Figure 4.1 presents the transmissibility of sub-frame accelerations relative to the vehicle body, for one representative vehicle. The results indicate that the sub-frame not only presents vertical oscillations but also significant rotational (pitch) behavior, as indicated by frequency-dependent variations in both the amplitude and phase between the two measurement points. Similar vibrational behavior was found in the other two vehicles as well.

The interaction of the sub-frame with the PWT was not analyzed, as only a single accelerometer was installed on the PWT.

4.2 Parameter estimation process

The parameter estimation process described in Section 3.5 was applied to determine the optimal vertical parameter values for each tested vehicle axle. Both the axle model and the transmissibility channels used for fitting are chosen according to the axle architecture in each case, resulting in a total of 6 sets of parameters.

Table 4.1 summarizes the corresponding estimation evaluation obtained. The highlighted `pad_to_body` transmissibility channel is the most relevant one, since it represents the transmissibility from a road input to the vehicle body.

Axle	**Percent of fit**			
	`pad_to_wheel`	`pad_to_PWT`	`pad_to_body`	**Average**
A	91%	83%	**87%**	87%
B	85%	71%	**79%**	78%
C	92%	-	**92%**	92%
D	90%	74%	**85%**	83%
E	82%	53%	**79%**	71%
F	92%	53%	**85%**	77%

Table 4.1: Parameter estimation evaluation percentages for each axle.

To exemplify the fitting percentages obtained, the resultant transmissibilities of the Axle E and F models will be shown in the following figures. The vehicle has an ICE powertrain on the front axle and an electric powertrain on the rear axle. Figures 4.2 and 4.3 compare the transmissibility of the model between pad and body, before and after the parameter estimation, and over the measurement. There are clear differences between front and rear axles, mostly influenced by the different powertrain weight and resonance frequency.

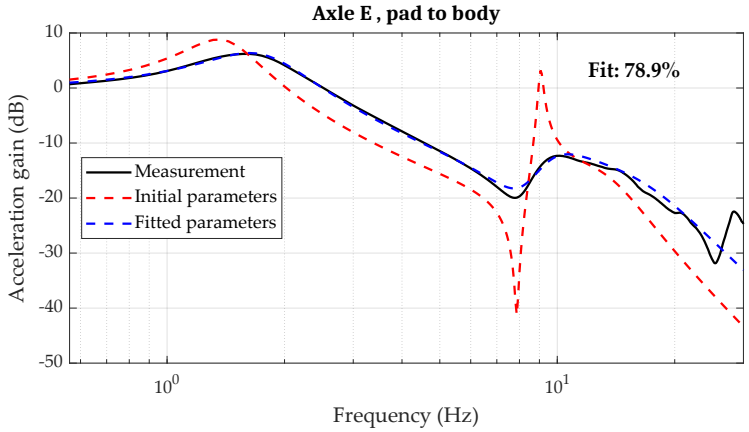

Figure 4.2: Axle E `pad_to_body` transmissibility before and after parameter estimation.

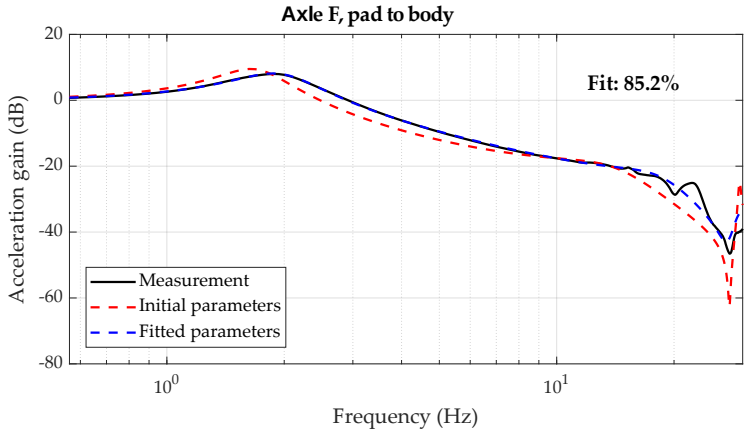

Figure 4.3: Axle F `pad_to_body` transmissibility before and after parameter estimation.

Figures 4.4 and 4.5 visualize the transmissibility between body and PWT, before and after the parameter estimation. The curves show notable differences between the ICE PWT of the front axle and the electric PWT of the rear axle. They also highlight how the real dynamics of these elements deviate from those of the simple spring-mass-damper system used in the model, resulting to a less accurate fit. Nonetheless, the model is able to capture the overall trend of the response.

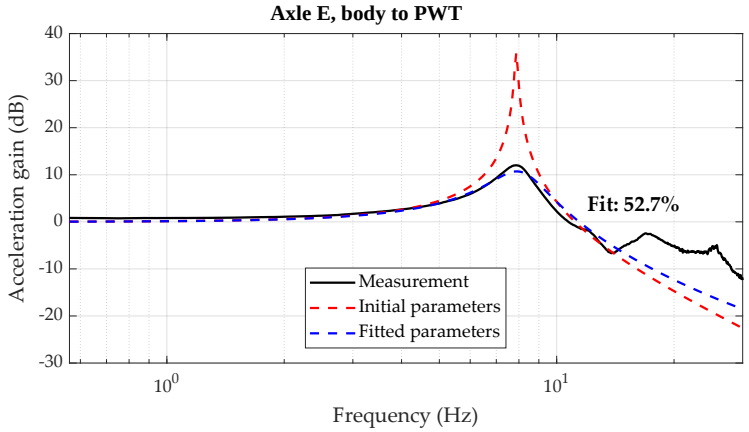

Figure 4.4: Axle E `body_to_PWT` transmissibility before and after parameter estimation.

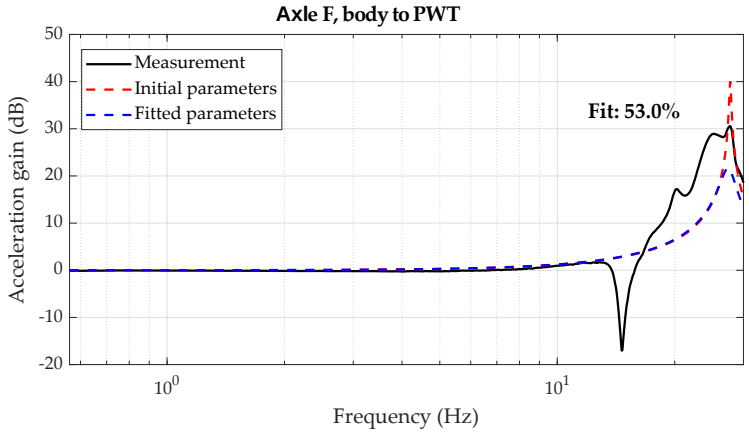

Figure 4.5: Axle F `body_to_PWT` transmissibility before and after parameter estimation.

4.3 Determined model parameters

The set of model parameters values was established by combining measured values using the K&C rig and initial educated guesses, based either on previous measurements of similar components for the masses or resonant frequency analysis for stiffness values such as the PWT stiffness. Furthermore, optimized values from the parameter estimation process were obtained for the vertical and tire parameters.

Each parameter table corresponds to a specific axle model, which has an associated configuration. This results in some parameters being missing for some models, such as motion ratios or sub-frame stiffness. The parameters description is available in Table 3.1, it is important to note that all the values listed correspond to a vehicle corner level, not to the complete axle.

	Parameter	Unit	Fitted
Masses	Corner total mass	kg	No
	Unsprung mass	kg	Yes
	TM mass	kg	No
	PWT mass	kg	Yes
Vertical	Wheel to body stiffness	N/m	Yes
	Wheel to body damping	Ns/m	Yes
	TM stiffness	N/m	Yes
	TM damping	Ns/m	Yes
	PWT stiffness	N/m	Yes
	PWT damping	Ns/m	Yes
Longitudinal	Wheel to body stiffness	N/m	No
	Wheel to body damping	Ns/m	No
	PWT stiffness	N/m	No
	PWT damping	Ns/m	No
Tire	Tire stiffness	N/m	Yes
	Tire damping	Ns/m	Yes
	Tire unloaded radius	m	No
	Tire static load	N	No
	Tire static deflection	m	No

Table 4.2: Axle A model parameters table, corner-level values

	Parameter	Unit	Fitted
Masses	Corner total mass	kg	No
	Unsprung mass	kg	Yes
	TM mass	kg	No
	PWT mass	kg	Yes
Vertical	Wheel to body stiffness	N/m	Yes
	Wheel to body damping	Ns/m	Yes
	TM stiffness	N/m	Yes
	TM damping	Ns/m	Yes
	PWT stiffness	N/m	Yes
	PWT damping	Ns/m	Yes
	Spring motion ratio	–	No
	Damper motion ratio	–	No
Longitudinal	Wheel to body stiffness	N/m	No
	Wheel to body damping	Ns/m	No
	SF stiffness	N/m	No
	SF damping	Ns/m	No
	PWT stiffness	N/m	No
	PWT damping	Ns/m	No
Tire	Tire stiffness	N/m	Yes
	Tire damping	Ns/m	Yes
	Tire unloaded radius	m	No
	Tire static load	N	No
	Tire static deflection	m	No

Table 4.3: Axle B model parameters table, corner-level values

	Parameter	Unit	Fitted
Masses	Corner total mass	kg	No
	Unsprung mass	kg	Yes
	TM mass	kg	No
Vertical	Wheel to body stiffness	N/m	Yes
	Wheel to body damping	Ns/m	Yes
	TM stiffness	N/m	Yes
	TM damping	Ns/m	Yes
Longitudinal	Wheel to body stiffness	N/m	No
	Wheel to body damping	Ns/m	No
Tire	Tire stiffness	N/m	Yes
	Tire damping	Ns/m	Yes
	Tire unloaded radius	m	No
	Tire static load	N	No
	Tire static deflection	m	No

Table 4.4: Axle C model parameters table, corner-level values

	Parameter	Unit	Fitted
Masses	Corner total mass	kg	No
	Unsprung mass	kg	Yes
	TM mass	kg	No
	SF mass	kg	No
	PWT mass	kg	Yes
Vertical	Wheel to body stiffness	N/m	Yes
	Wheel to body damping	Ns/m	Yes
	TM stiffness	N/m	Yes
	TM damping	Ns/m	Yes
	PWT stiffness	N/m	Yes
	PWT damping	Ns/m	Yes
	Spring motion ratio	–	No
	Damper motion ratio	–	No
Longitudinal	Wheel to body stiffness	N/m	No
	Wheel to body damping	Ns/m	No
	SF stiffness	N/m	No
	SF damping	Ns/m	No
	PWT stiffness	N/m	No
	PWT damping	Ns/m	No
Tire	Tire stiffness	N/m	Yes
	Tire damping	Ns/m	Yes
	Tire unloaded radius	m	No
	Tire static load	N	No
	Tire static deflection	m	No

Table 4.5: Axle D model parameters table, corner-level values

	Parameter	Unit	Fitted
Masses	Corner total mass	kg	No
	Unsprung mass	kg	Yes
	TM mass	kg	No
	PWT mass	kg	Yes
Vertical	Wheel to body stiffness	N/m	Yes
	Wheel to body damping	Ns/m	Yes
	TM stiffness	N/m	Yes
	TM damping	Ns/m	Yes
	PWT stiffness	N/m	Yes
	PWT damping	Ns/m	Yes
	Spring motion ratio	–	No
	Damper motion ratio	–	No
Longitudinal	Wheel to body stiffness	N/m	No
	Wheel to body damping	Ns/m	No
	SF stiffness	N/m	No
	SF damping	Ns/m	No
	PWT stiffness	N/m	No
	PWT damping	Ns/m	No
Tire	Tire stiffness	N/m	Yes
	Tire damping	Ns/m	Yes
	Tire unloaded radius	m	No
	Tire static load	N	No
	Tire static deflection	m	No

Table 4.6: Axle E model parameters table, corner-level values (sanitized).

	Parameter	Unit	Fitted
Masses	Corner total mass	kg	No
	Unsprung mass	kg	Yes
	TM mass	kg	No
	SF mass	kg	No
	PWT mass	kg	Yes
Vertical	Wheel to body stiffness	N/m	Yes
	Wheel to body damping	Ns/m	Yes
	TM stiffness	N/m	Yes
	TM damping	Ns/m	Yes
	PWT stiffness	N/m	Yes
	PWT damping	Ns/m	Yes
	Spring motion ratio	–	No
	Damper motion ratio	–	No
Longitudinal	Wheel to body stiffness	N/m	No
	Wheel to body damping	Ns/m	No
	SF stiffness	N/m	No
	SF damping	Ns/m	No
	PWT stiffness	N/m	No
	PWT damping	Ns/m	No
Tire	Tire stiffness	N/m	Yes
	Tire damping	Ns/m	Yes
	Tire unloaded radius	m	No
	Tire static load	N	No
	Tire static deflection	m	No

Table 4.7: Axle F model parameters table, corner-level values (sanitized).

4.4 Model evaluation with track measurements

4.4.1 Vehicle body accelerations

Figures 4.6, 4.7 and 4.8 compare the simulated body vertical and longitudinal accelerations with the vehicle measurements from the Cleat test, as described in Section 3.4.3. A cleat height of 30mm and a test velocity of 30km/h have ben chosen as the most representative scenario and so it is the case shown in the plots. The rest of the cases are analyzed in the following Section 4.4.2.

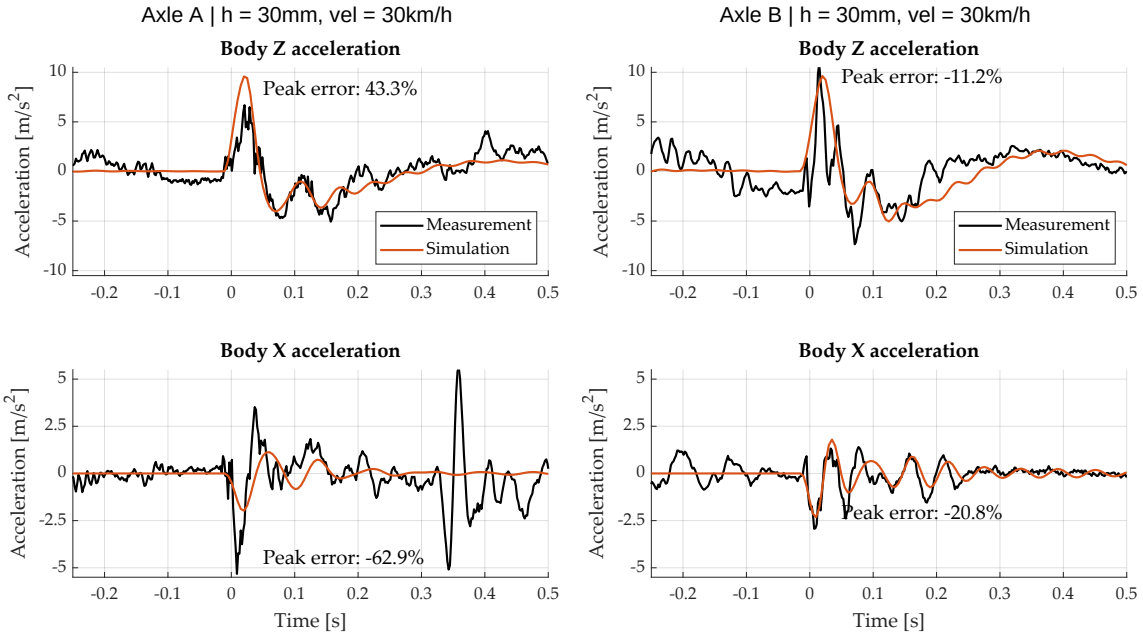

Figure 4.6: Measured and simulated body accelerations of the first vehicle tested.

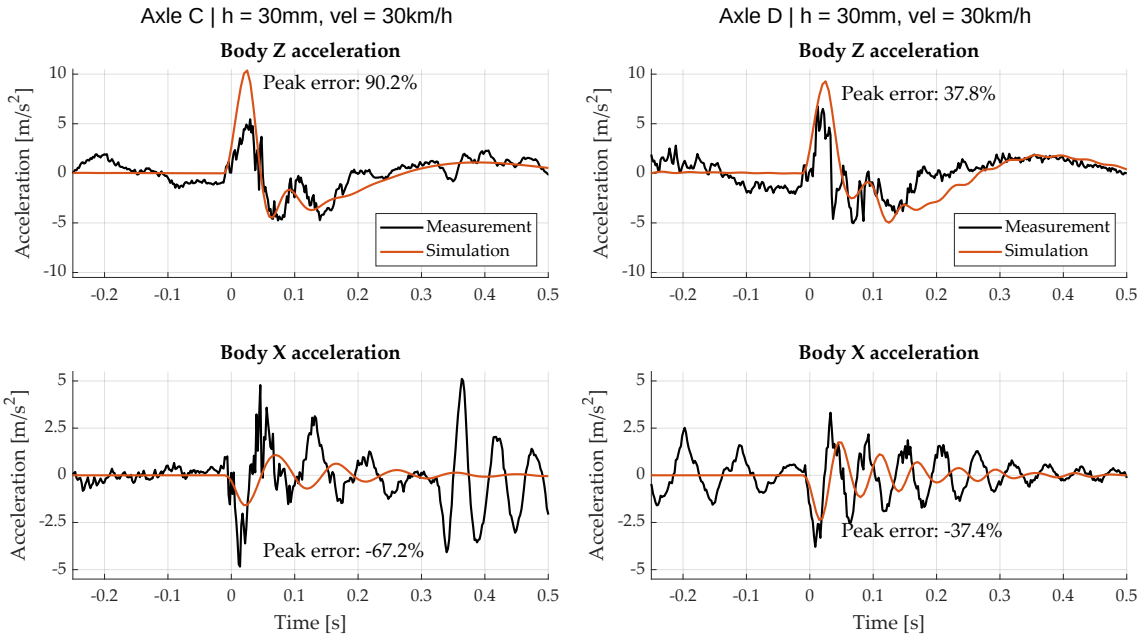

Figure 4.7: Measured and simulated body accelerations of the second vehicle tested.

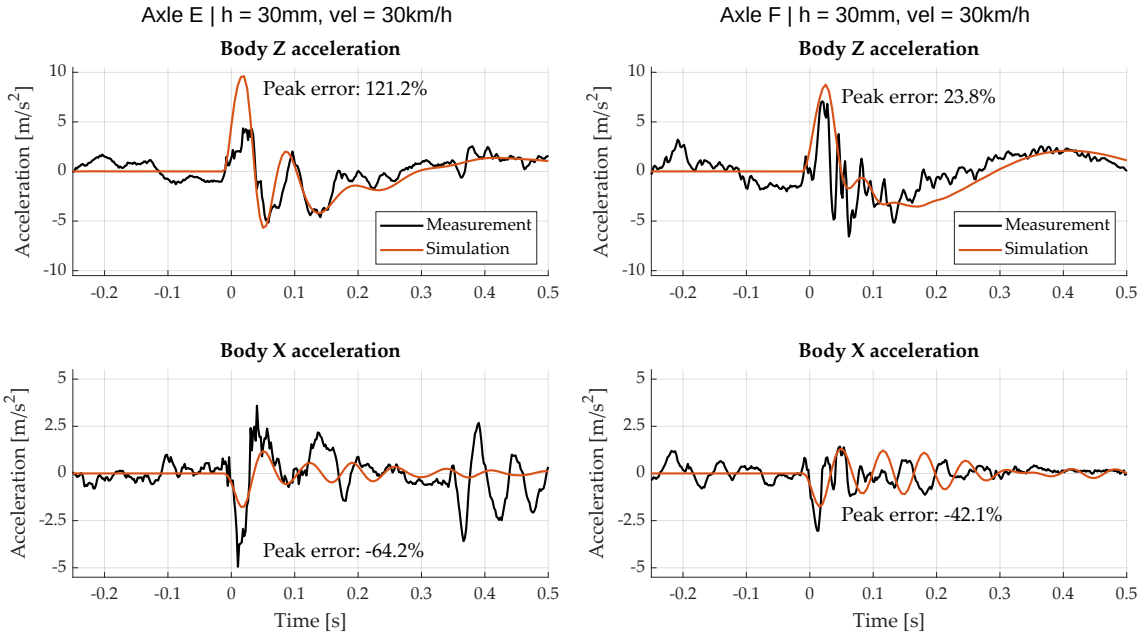

Figure 4.8: Measured and simulated body accelerations of the third vehicle tested.

4.4.2 Complete dataset analysis

In order to visualize all the test conditions, the peak error and after-shake error metrics described in Section 3.6.2 have been computed for each case. The resultant relative error values are presented in the histograms in Figure 4.9, 4.10, 4.11 and 4.12, for both vertical and longitudinal accelerations.

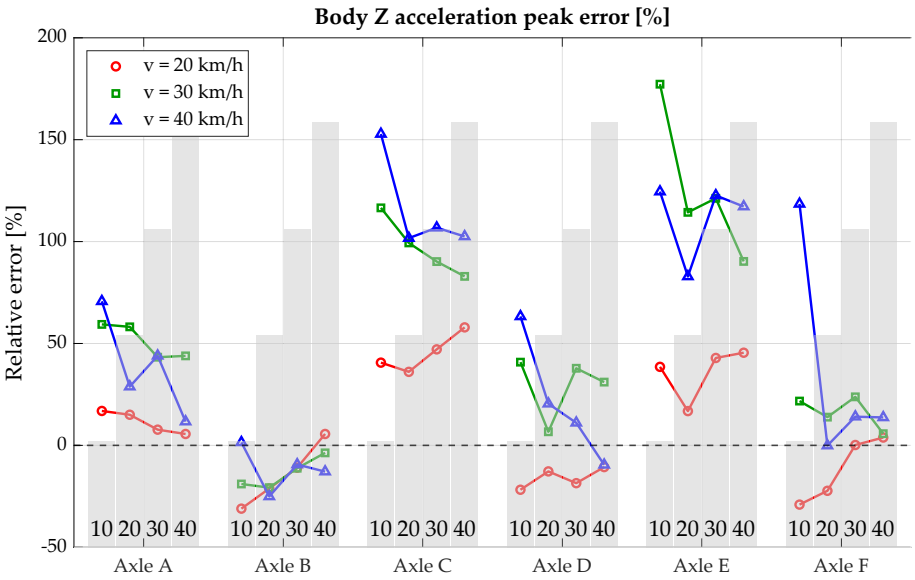

Figure 4.9: Body Z-axis peak acceleration relative error for varying cleat heights (10, 20, 30, 40 mm) and test velocities, organized by axle.

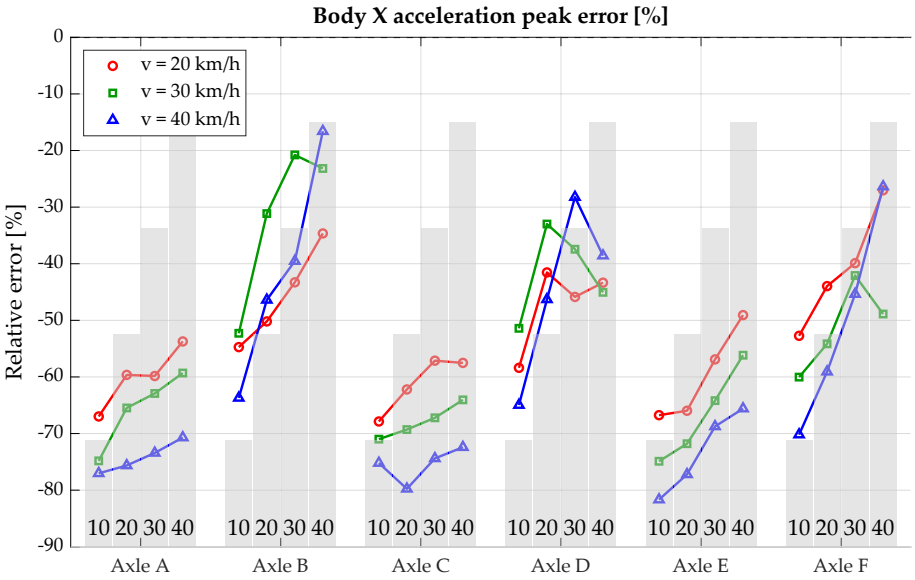

Figure 4.10: Body X-axis peak acceleration relative error for varying cleat heights (10, 20, 30, 40 mm) and test velocities, organized by axle.

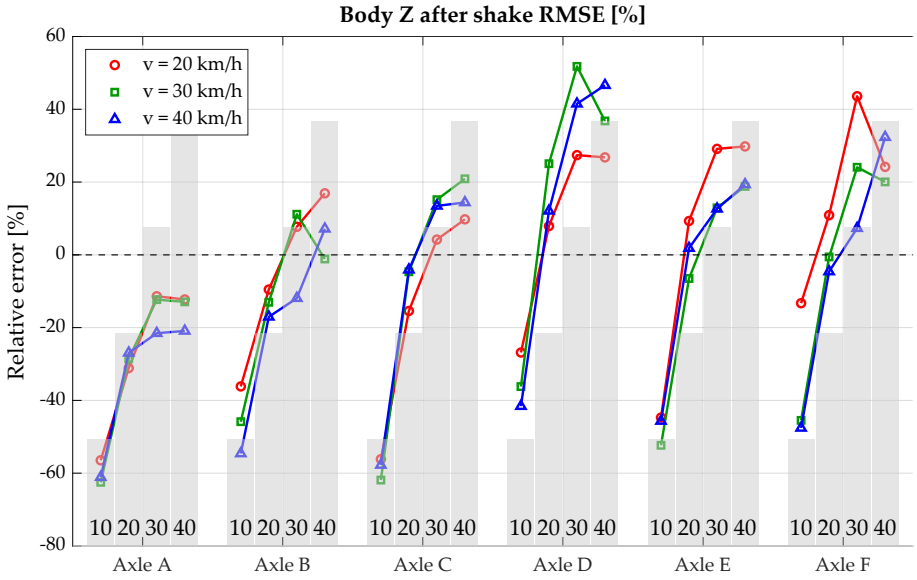

Figure 4.11: Body Z-axis after shake RMS relative error for varying cleat heights (10, 20, 30, 40 mm) and test velocities, organized by axle.

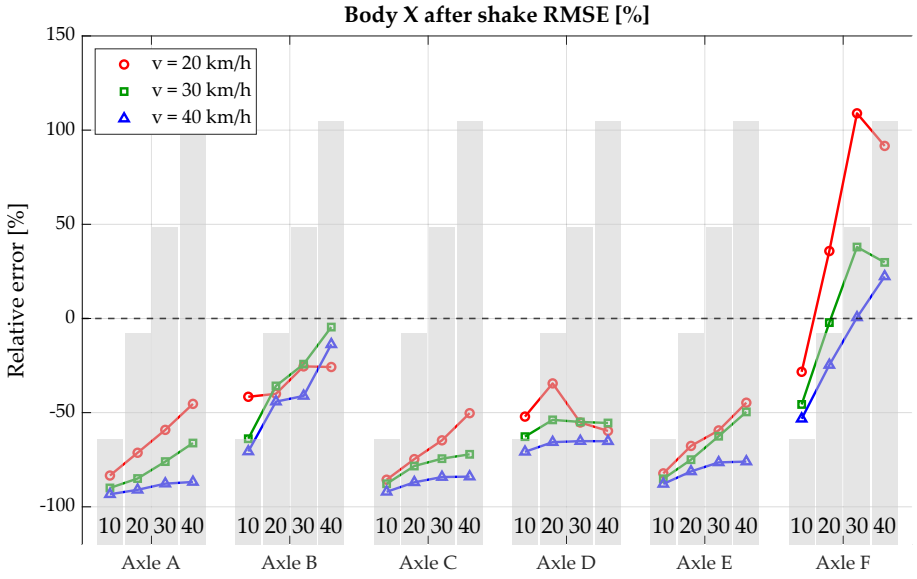

Figure 4.12: Body X-axis after shake RMS relative error for varying cleat heights (10, 20, 30, 40 mm) and test velocities, organized by axle.

4.4.3 Model analysis

4.4.3.1 Influence of longitudinal and tire sub-models on body accelerations

The two model variants described in Section 3.6.3 were simulated and compared against the complete model. The first variant is a longitudinally-locked model, which includes only the tire model and the vertical suspension dynamics. The second variant uses a simplified point-contact tire model, again including only the vertical dynamics. Figure 4.13 presents the body and wheel vertical accelerations for all three model configurations. These results will be discussed in detail in Section 5.3.2.

It is worth noting that the differences between the longitudinally-locked and the complete model variants are marginal. However, time alignment varies slightly due to the peak wheel acceleration happening slightly earlier in the longitudinally-locked variant.

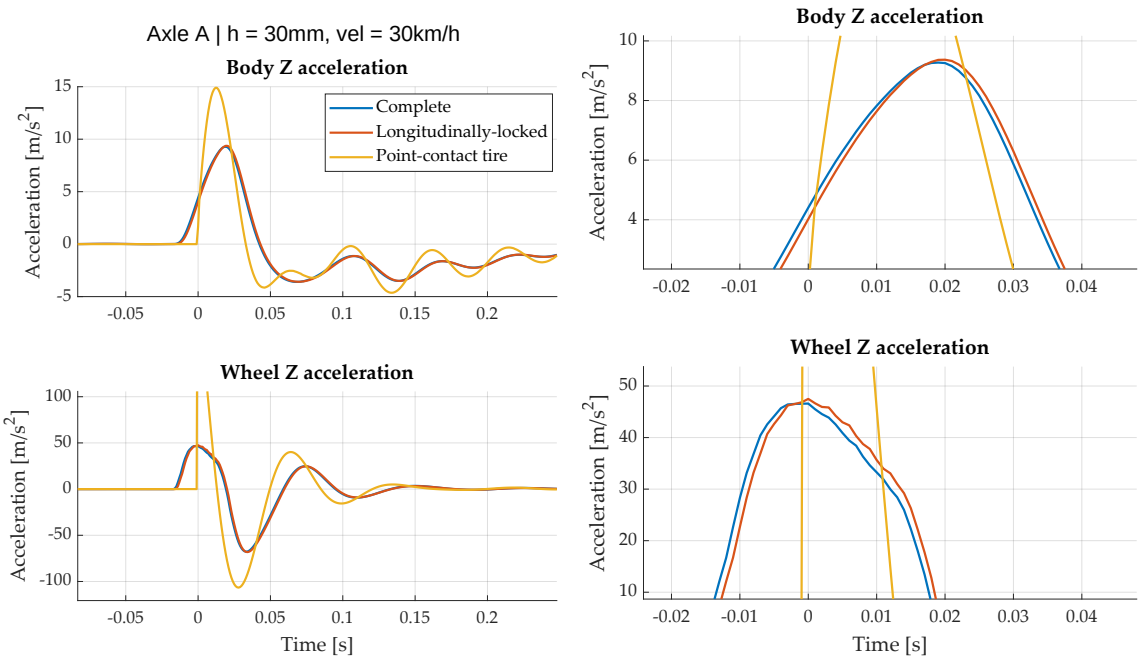

Figure 4.13: Comparison of model variants, including a zoomed-in view.

4.4.3.2 Tire model analysis

Wheel accelerations have been analyzed to estimate the discrepancy between the forces generated by the actual tire and those predicted by the model. However, this approach provides only an approximation, as the measured wheel accelerations are also influenced by the forces transmitted through the suspension elements—specifically, the vertical spring and damper, as well as the longitudinal bushing. As a result, the accelerations do not directly correspond to the tire forces, although they are dominated by the stiffer tire dynamics at the initial time steps of the cleat impact. Figures 4.14, 4.15 and 4.16 compare the simulated and measured wheel accelerations—both vertical and longitudinal—for each of the measured axles.

An additional simulation was conducted using unrealistically low longitudinal wheel stiffness, to further isolate the tire-generated forces within the model. The resulting accelerations are shown in Figure 4.17, while Figure 4.18 compares the forces from both the tire and the longitudinal suspension. The significantly lower magnitude of the suspension forces confirms the effectiveness of the isolation.

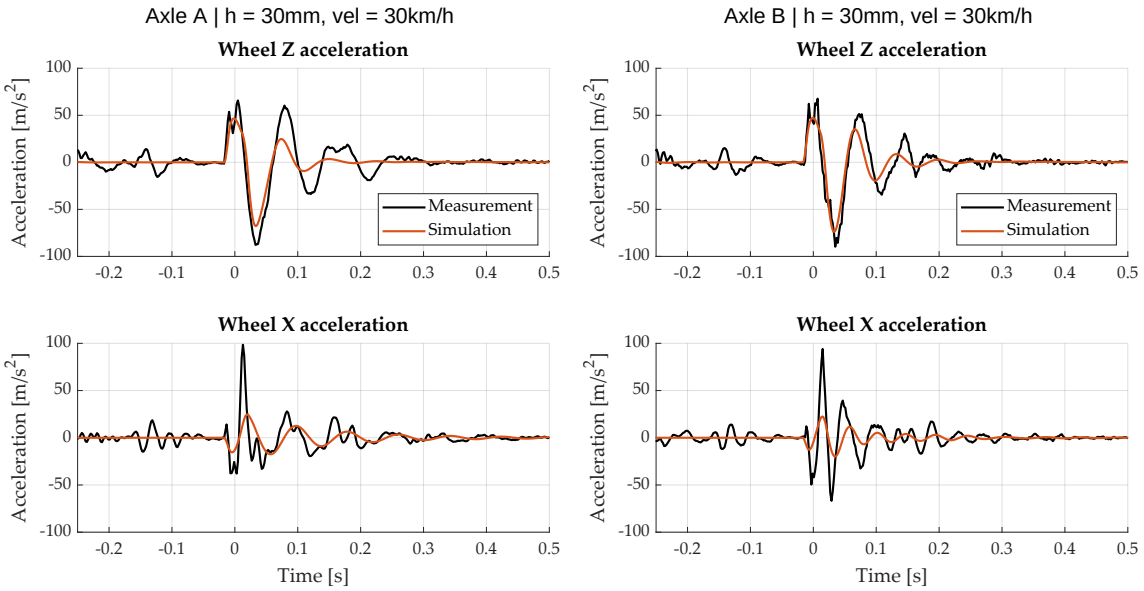

Figure 4.14: Measured and simulated wheel accelerations of the first vehicle tested.

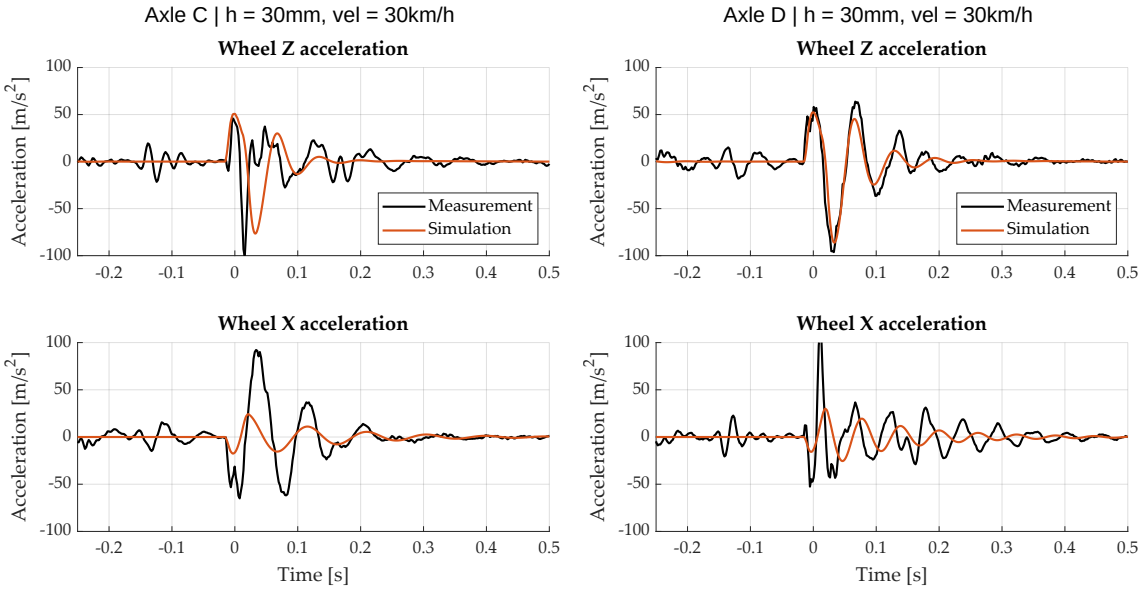

Figure 4.15: Measured and simulated wheel accelerations of second vehicle tested.

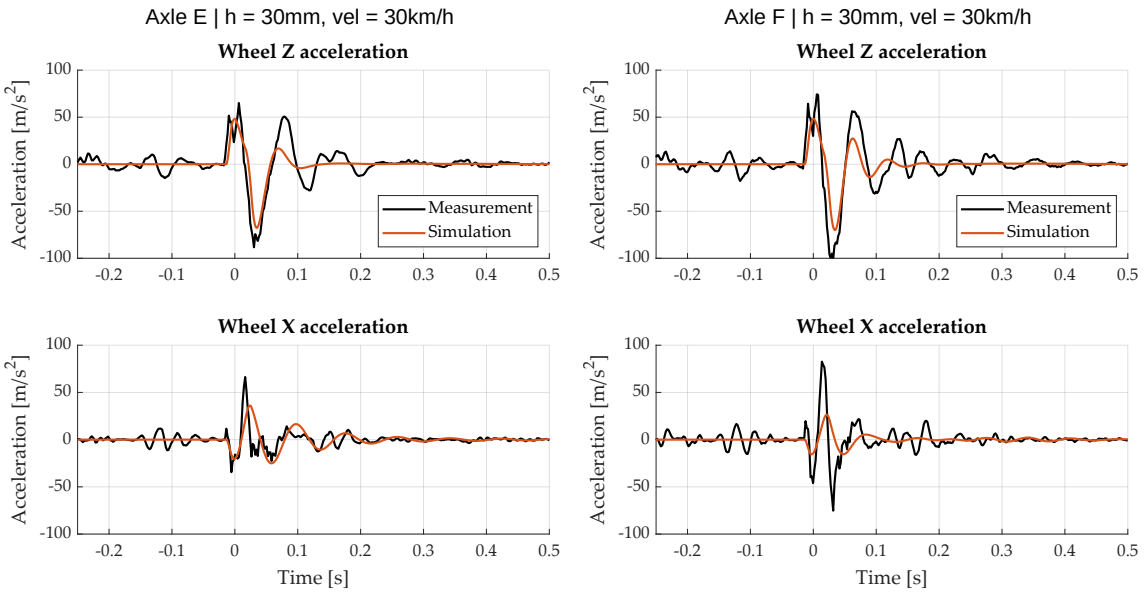

Figure 4.16: Measured and simulated wheel accelerations of the third vehicle tested.

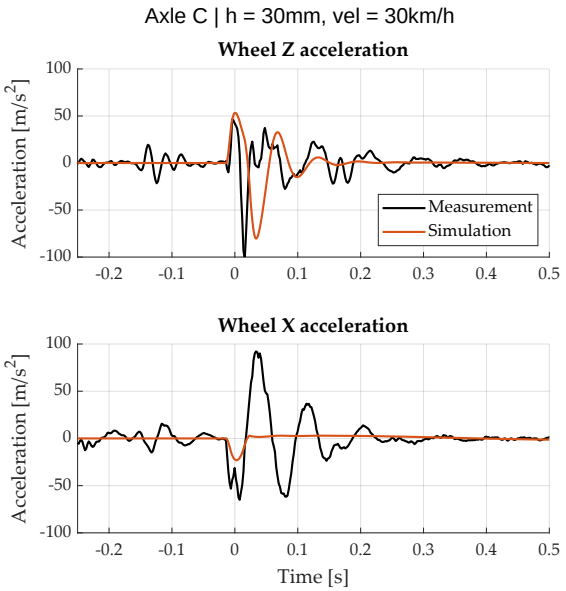

Figure 4.17: Wheel accelerations of the Axle C with unrealistically low longitudinal stiffness.

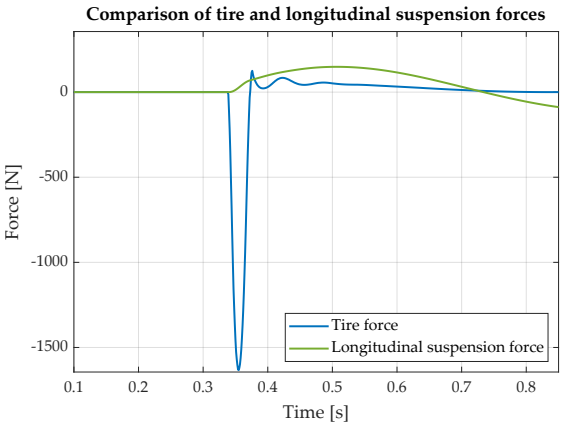

Figure 4.18: Longitudinal forces affecting the wheel.

The same peak acceleration error metric used in the body acceleration analysis in Section 4.4.2 was applied to the wheel accelerations, in order to assess how the discrepancy varied with different axle parameters and cleat magnitudes. The results are presented in the histograms shown in Figures 4.19 and 4.21, which display the wheel peak acceleration errors for the complete dataset.

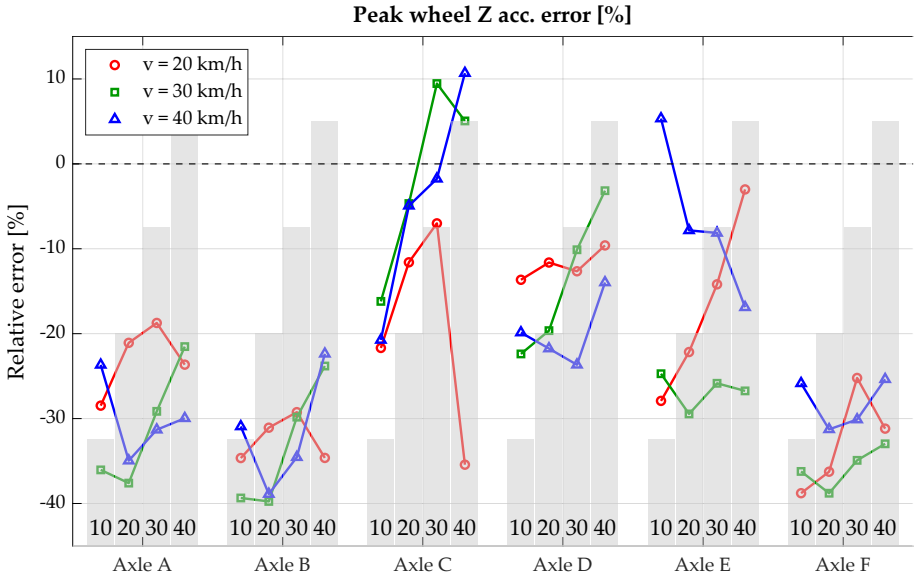

Figure 4.19: Wheel Z-axis peak acceleration relative error for varying cleat heights (10,20,30,40 mm) and test velocities, organized by axle.

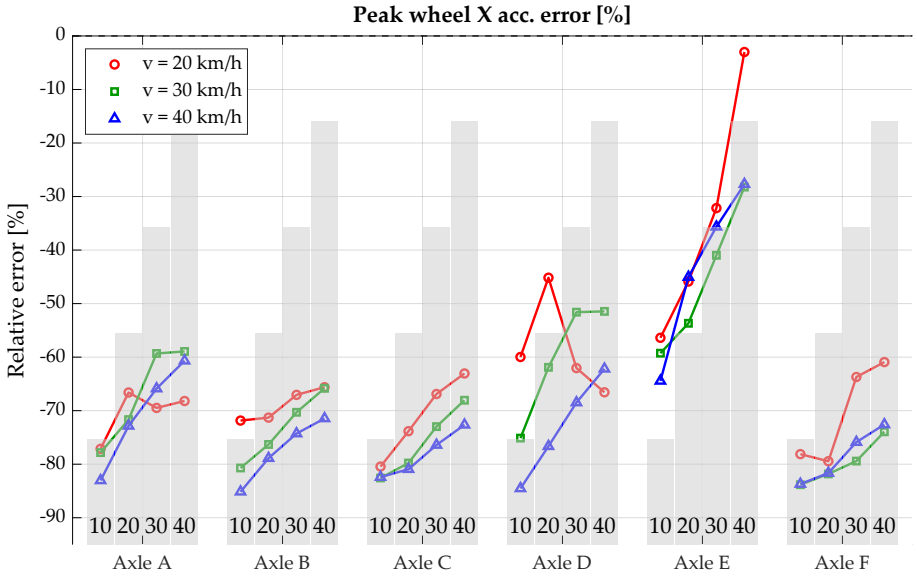

Figure 4.20: Wheel X-axis peak acceleration relative error for varying cleat heights (10,20,30,40 mm) and test velocities, organized by axle.

4.5 Python tool

A tool was built in which the user enters vehicle information, including axle configuration and initial model parameter guesses, via an Excel file. The tool then performs parameter estimation through optimization and presents the results in a graphical user interface, displaying the fitted parameters alongside transmissibility plots that illustrate the quality of the curve fits.

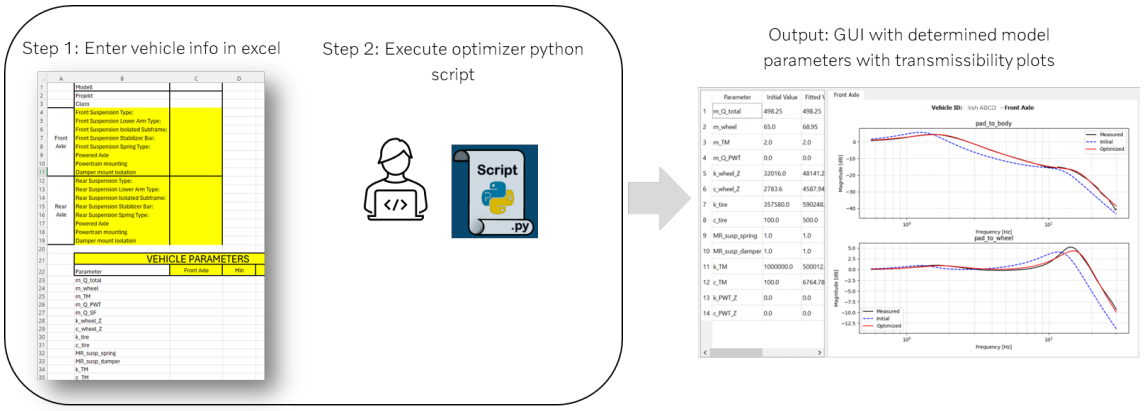

Figure 4.21: Parameter estimation tool

.

5

Discussion

5.1 Sub-frame measurement difficulties

Analyzing the sub-frame (SF) displacements proved more complex than initially anticipated. Measurements from the setup described in Section 3.4.2 revealed that the SF does not follow a straight longitudinal path when a longitudinal force is applied at the wheel center. This behavior results from a combination of anti-squat suspension geometry—which applies some portion of the longitudinal force vertically—and the vertical distance between the wheel center and the SF bushings, which introduces a moment at the SF, inducing a rotation. The combination of these effects required simplifications to approximate a constant SF longitudinal stiffness.

Furthermore, as shown in Section 4.1, Shake Rig measurements revealed rotational vibration modes in the SF. These dynamic behaviors introduce additional complexity to the parameter estimation process, which is further discussed in Section 4.1.

5.2 Parameter estimation process

After several iterations, the parameter estimation process performed well, driven by the cost function described in Section 3.5.2.1, successfully converging to reasonable solutions across all measured axles. Nevertheless, throughout the development process a number of challenges and considerations emerged.

5.2.1 Difficulties estimating sub-frame parameters

Attempts to obtain reasonable estimated parameters for the sub-frame (SF) and powertrain (PWT)—specifically stiffness and damping—were ultimately unsuccessful due to several reasons. Firstly, the model does not account for the rotational vibration modes identified in the measurements, which were analyzed in Section 4.1. Additionally, the center of gravity (CoG) of the PWT is unknown, which implies that the relative position of the vertical accelerometers with respect to the CoG is also unknown. As a result, the measured accelerations do not accurately reflect the vertical oscillations of the PWT mass at its CoG.

The parameter identification process was also limited by the local optimization algorithm, which tended to converge to a local minimum with unrealistically high

stiffness values. This often resulted in the SF appearing to be rigidly locked to the body, or the PWT locked to the SF.

A secondary approach was explored in which the SF mass was retained in the model, but direct optimization against SF-related channels (e.g., `body_to_SF` and `PWT_to_SF`) was omitted. Instead, optimization relied on the `body_to_PWT` transmissibility, under the assumption that SF dynamics would still influence the observed PWT motion. In practice, this method did not yield consistent or physically reasonable SF parameter values, as the contributions of SF stiffness and damping could not be uniquely separated from those of the PWT mounts.

To address these limitations, the model was ultimately simplified by removing the SF mass and representing both SF and PWT with a single PWT mass. This single resonating mass was sufficient to capture the dominant damping effects on the vehicle body, while avoiding the complexities introduced by the intermediate SF dynamics.

5.2.2 Local optimization limitations

Different parameter combinations can achieve good curve fitting. However, with the current local optimization algorithm, the process stops once a local minimum is found, potentially concluding a parameter set that might differ from a more physically realistic solution. Using a global optimization method could help explore a wider range of parameter sets, minimizing the initial parameter sensitivity, and enabling for the selection of a final parameter set based on specific criteria.

5.2.3 Quarter Car equivalent mass assumption as a source of error and potential improvements

The Quarter Car equivalent mass approximation presented in Section 2.3.1 is often an overlooked parameter. It is treated as a constant value in the parameter estimation process, implying a fixed body apparent mass or inertia acting on the excited axle. However, this approximation is likely inaccurate, since in reality the apparent mass depends on the vehicle body's moment of inertia around the Y-axis (pitch axis), and the instantaneous pitch center, which itself is influenced by the suspension stiffness of the non-exited axle.

This variability has not been quantified, so the extent of the resulting error remains unknown. To illustrate the potential impact, consider a hypothetical chassis with a very high pitch inertia and a very short wheelbase. In such a case, the dynamic apparent mass at each axle would approach the total vehicle mass, rendering the Quarter Car simplification invalid.

A suggested solution is to use a second accelerometer in the non-excited axle. This would allow the estimation of the instantaneous pitch center's longitudinal (X-axis) position, based on front and rear vertical accelerations. Combined with the pitch moment of inertia—measurable using the Kinematics & Compliance (K&C) rig—the apparent axle mass could be estimated.

A more advanced alternative would be to expand the model to a single-track representation, combining front and rear corner models. This would eliminate the need for approximating the body mass altogether, allowing for a more accurate and physically representative simulation.

5.3 Model analysis

The response discrepancies observed in the results presented in Section 4.4 have been further analyzed to roughly quantify the contribution of each model subsystem to the overall error. The modular structure of the model significantly facilitated the analysis by enabling the generation of model variants that isolate the dynamic effects of the longitudinal suspension and the tire model. These two components constitute the main addition over a conventional pure vertical quarter-car model.

5.3.1 Tire model limitations

The wheel accelerations presented in Section 4.4.3.2 reveal a consistent underestimation of the longitudinal force generated by the tire, regardless of the axle parameters used. This observation is further supported by the simulation using an artificially reduced longitudinal wheel stiffness—effectively isolating the tire's longitudinal force contribution. As shown in Figure 4.17, the tire model's longitudinal force is not sufficient to accelerate the wheel, even in the absence of the reaction force from the longitudinal suspension.

These results indicate that the effective stiffness of the real tire under the cleat impact conditions—characterized by a high frequency content—must be significantly higher to reproduce the observed accelerations. This behavior suggests that a nonlinear stiffness is needed in the tire model to be able to capture the response.

5.3.2 Contribution of the longitudinal suspension and tire models

The responses of the longitudinally-locked and the purely vertical model variants are presented in Figure 4.13. The most immediate observation is that constraining the longitudinal dynamics has minimal effect on the vertical accelerations. In contrast, the purely vertical model—which uses the point-contact tire model—shows a significant discrepancy, particularly in the wheel vertical acceleration. This indicates that the tire model has a far greater influence on the model response than the longitudinal suspension dynamics.

However, a key consideration lies in the previously discussed limitations of the tire model. The underestimation of longitudinal suspension excitation—relative to the vertical—may reduce the influence of longitudinal wheel motion on vertical accelerations, explaining why the complete model response appears largely unaffected by longitudinal dynamics. In reality, if the rearward displacement of the wheel were larger—as suggested by acceleration measurements—the average relative velocity

between the wheel and the cleat during the impact event would be reduced in both vertical and longitudinal components. This, in turn, would lower the vertical wheel velocity and acceleration, ultimately reducing the vertical force transmitted to the body through the main suspension spring and damper, and thereby lowering the resulting body vertical acceleration.

6

Conclusion

The study set out to examine whether a simplified modeling approach could provide meaningful guidance for impact harshness target setting early in the vehicle development process. The results demonstrate that the model is capable of reproducing key vertical oscillations and, through rig-based parameter estimation, successfully captured the vehicle's vertical dynamic stiffness within the 0–30 Hz range. This result indicates that the approach can provide useful insights for early ride comfort evaluations, where efficiency and accessibility are important.

At the same time, the limitations of the combined vertical–longitudinal framework were evident. Missing tire high-frequency stiffness and unrepresentative longitudinal parameters led to consistent underestimation of longitudinal forces relative to vertical ones, resulting in inaccurate tire force magnitudes and angles during cleat events. Nonlinear and higher-order effects, though expected, further added to the model error and highlighted the constraints of linear approximations.

Overall, the thesis demonstrates that while simplified models cannot fully substitute for detailed simulations or physical validation, they can bridge the gap in the early design phase by offering a reliable foundation for vertical ride target setting. With further refinement in tire modeling and inclusion of nonlinear dynamics, the approach holds promise for broader application in capturing both vertical and longitudinal ride behaviors.

6.1 Future Work

The simplified quarter-car approach adopted in this thesis proved effective for exploring vertical ride dynamics, but it also introduced clear limitations. Because accelerations were recorded one axle at a time, the apparent mass in the model was treated as a single constant, rather than reflecting full-body effects. A natural extension would therefore be to expand the model to a one-track vehicle representation. Using full-body excitation in the shaker rig, combined with accelerometers at both the front and rear, would make it possible to estimate the body apparent mass and pitch moment of inertia, as outlined in the referenced PhD work [15]. This would allow the model to simulate both primary and secondary ride events, while still being limited to symmetric input conditions.

The model could also benefit from incorporating nonlinearities. Incorporating non-

linear damping would allow a more realistic representation of amplitude-dependent behavior. Incorporating frictional effects could also enhance model fidelity. The thesis[3] may serve as a useful reference for assessing the significance of friction in this context, particularly once nonlinear elements are introduced.

Finally, future work should address the representation of bushing dynamics. Including nonlinear stiffness and saturation effects would improve the model's ability to capture realistic component behavior. It would also be valuable to investigate how combined vertical and longitudinal deformations influence saturation thresholds, as these interactions may cause the bushing to reach limits at lower loads than when each deformation occurs independently.

Bibliography

[1] Y. Huang, "Target-driven road vehicle suspension design," Licentiate thesis, Chalmers Univ. Technol., 2019.

[2] J. R. Cho, K. W. Kim, D. H. Jeon, and W. S. Yoo, "Transient dynamic response analysis of 3-D patterned tire rolling over cleat," *International Journal of Mechanical Sciences*, vol. 250, 2023, Art. no. 108428. http://dx.doi.org/10.1016/j.euromechsol.2005.01.004

[3] O. Jonson and E. Enders, *Correlation Work on Shaker Rig Tests and Simulations: An investigation of damper, bushing, friction and tire modeling with respect to vertical vibration insulation*, Master's thesis, Chalmers University of Technology, Gothenburg, Sweden, 2020.

[4] Bakirci, I. and Katadzic, N. (2014). The use of wheel torque modulation to mitigate road induced longitudinal vibrations.

[5] The Shock Absorber Handbook by John C. Dixon

[6] B. Jacobsson, *Axle and Wheel Rates*, in *Compendium in Vehicle Motion Engineering*, Chalmers University of Technology, 2024, pp. 187-188.

[7] Jian Jun Zhu, Amir Khajepour, Ebrahim Esmailzadeh & Alireza Kasaiezadeh (2012). Ride quality evaluation of a vehicle with a planar suspension system, Vehicle System Dynamics, 50:3, 395-413.

[8] Reza N. Jazar (2014). *Vehicle Dynamics: Theory and Application*, 2nd Edition, Springer.

[9] AB Dynamics. *Kinematics & Compliance Test Equipment.* Available at: `https://www.abdynamics.com/lab-testing/kinematics-compliance-test-equipment/` [Accessed: DATE].

[10] Multimatic. *Multi-Post Rig Testing.* Available at: `https://www.multimatic.com/engineering/testing/multi-post-testing`

[11] T. D. Gillespie, *Fundamentals of Vehicle Dynamics.* Warrendale, PA: SAE International, 1992.

[12] B. Heissing and M. Ersoy, *Chassis Handbook: Fundamentals, Driving Dynamics, Components, Mechatronics, Perspectives.* Wiesbaden: Vieweg+Teubner,

2011.

[13] M. J. Griffin, *Handbook of Human Vibration*. London: Academic Press, 1990.

[14] M. W. Neal, W. Cwycyshyn, and I. Badiru, "Tuning dampers for ride and handling of production vehicles," 2015. DOI: https://doi.org/10.4271/2015-01-1589.

[15] L. J. Bennett, *Ride and handling assessment of vehicles using four-post rig testing and simulation*, PhD Thesis, Oxford Brookes University, 2012.

[16] A. Brandt, *Noise and Vibration Analysis: Signal Analysis and Experimental Procedures*. John Wiley & Sons, 2011.

[17] Y. Cui, T. R. Kurfess, and M. Messman, *Testing and Modeling of Nonlinear Properties of Shock Absorbers for Vehicle Dynamics Studies*, *Mechanical Systems and Signal Processing*, vol. 24, no. 3, pp. 850–863, 2010.

[18] Wikipedia contributors. *Viscoelasticity* — Wikipedia, The Free Encyclopedia. Available at: https://en.wikipedia.org/wiki/Viscoelasticity. Accessed: July 7, 2025.

[19] J. E. Dennis Jr., "Nonlinear least squares and equations," in *Scientific Computing: Proceedings of the Symposium on Scientific Computing*, pp. 43–61, 1977.

[20] D. C. Davis, "A radial-spring terrain-enveloping tire model," *Vehicle System Dynamics*, vol. 4, no. 1, pp. 55–69, 1975. https://doi.org/10.1080/00423117508969453

DEPARTMENT OF MECHANICS AND MARITIME SCIENCES
CHALMERS UNIVERSITY OF TECHNOLOGY
Gothenburg, Sweden 2025
www.chalmers.se

CHALMERS
UNIVERSITY OF TECHNOLOGY